ENGINEERING OF
BIOMATERIALS

INŻYNIERIA BIOMATERIAŁÓW

ENGINEERING OF
BIO MATERIALS

ENGINEERING OF BIOMATERIALS

Wskazówki dla autorów

1. Prace do opublikowania w kwartalniku „Engineering of Biomaterials / Inżynieria Biomateriałów" przyjmowane będą wyłącznie w języku angielskim.

2. Wszystkie nadsyłane artykuły są recenzowane.

3. Materiały do druku prosimy przysyłać za pomocą systemu online (www.biomaterials.pl).

4. Struktura artykułu:
• TYTUŁ • Autorzy i instytucje • Streszczenie (200-250 słów) • Słowa kluczowe (4-6) • Wprowadzenie • Materiały i metody • Wyniki i dyskusja • Wnioski • Podziękowania • Piśmiennictwo

5. Autorzy przesyłają pełną wersję artykułu, łącznie z ilustracjami, tabelami, podpisami i literaturą w jednym pliku. Artykuł w tej formie przesyłany jest do recenzentów. Dodatkowo autorzy proszeni są o przesłanie materiałów ilustracyjnych (rysunki, schematy, fotografie, wykresy) w oddzielnych plikach (format np. .jpg, .gif., .tiff, .bmp). Rozdzielczość rysunków min. 300 dpi. Wszystkie rysunki i wykresy powinny być czarno-białe lub w odcieniach szarości i ponumerowane cyframi arabskimi. W tekście należy umieścić odnośniki do rysunków i tabel. W przypadku artykułów dwujęzycznych w tabelach i na wykresach należy umieścić opisy polskie i angielskie.

6. Na końcu artykułu należy podać wykaz piśmiennictwa w kolejności cytowania w tekście i kolejno ponumerowany.

7. Redakcja zastrzega sobie prawo wprowadzenia do opracowań autorskich zmian terminologicznych, poprawek redakcyjnych, stylistycznych, w celu dostosowania artykułu do norm przyjętych w naszym czasopiśmie. Zmiany i uzupełnienia merytoryczne będą dokonywane w uzgodnieniu z autorem.

8. Opinia lub uwagi recenzentów będą przekazywane Autorowi do ustosunkowania się. Nie dostarczenie poprawionego artykułu w terminie oznacza rezygnację Autora z publikacji pracy w naszym czasopiśmie.

9. Za publikację artykułów redakcja nie płaci honorarium autorskiego.

10. Adres redakcji:
Czasopismo
„Engineering of Biomaterials / Inżynieria Biomateriałów"
Akademia Górniczo-Hutnicza im. St. Staszica
Wydział Inżynierii Materiałowej i Ceramiki
al. Mickiewicza 30/A-3, 30-059 Kraków
tel. (48) 12 617 25 03, 12 617 25 61
tel./fax: (48) 12 617 45 41
e-mail: chlopek@agh.edu.pl, kabe@agh.edu.pl

Szczegółowe informacje dotyczące przygotowania manuskryptu oraz procedury recenzowania dostępne są na stronie internetowej czasopisma:
www.biomaterials.pl

Warunki prenumeraty

Zamówienie na prenumeratę prosimy przesyłać na adres:
mgr inż. Augustyn Powroźnik
apowroz@agh.edu.pl, tel/fax: (48) 12 617 45 41
Cena pojedynczego numeru wynosi 20 PLN
Konto: Polskie Stowarzyszenie Biomateriałów
30-059 Kraków, al. Mickiewicza 30/A-3
ING Bank Śląski S.A. O/Kraków
nr rachunku 63 1050 1445 1000 0012 0085 6001

Prenumerata obejmuje 4 numery regularne i nie obejmuje numeru specjalnego (materiały konferencyjne).

Instructions for authors

1. Papers for publication in quarterly journal „Engineering of Biomaterials / Inżynieria Biomateriałów" should be written in English.

2. All articles are reviewed.

3. Manuscripts should be submitted to editorial office through online submission system (www.biomaterials.pl).

4. A manuscript should be organized in the following order:
• TITLE • Authors and affiliations • Abstract (200-250 words) • Keywords (4-6) • Introduction • Materials and Methods • Results and Discussions • Conclusions • Acknowledgements • References

5. All illustrations, figures, tables, graphs etc. preferably in black and white or grey scale should be additionally sent as separate electronic files (format .jpg, .gif., .tiff, .bmp). High-resolution figures are required for publication, at least 300 dpi. All figures must be numbered in the order in which they appear in the paper and captioned below. They should be referenced in the text. The captions of all figures should be submitted on a separate sheet.

6. References should be listed at the end of the article. Number the references consecutively in the order in which they are first mentioned in the text.

7. The Editors reserve the right to improve manuscripts on grammar and style and to modify the manuscripts to fit in with the style of the journal. If extensive alterations are required, the manuscript will be returned to the authors for revision.

8. Opinion or notes of reviewers will be transferred to the author. If the corrected article will not be supplied on time, it means that the author has resigned from publication of work in our journal.

9. Editorial does not pay author honorarium for publication of article.

10. Address of editorial office:
Journal
„Engineering of Biomaterials / Inżynieria Biomateriałów"
AGH University of Science and Technology
Faculty of Materials Science and Ceramics
30/A-3, Mickiewicz Av., 30-059 Krakow, Poland
tel. (48) 12) 617 25 03, 12 617 25 61
tel./fax: (48) 12 617 45 41
e-mail: chlopek@agh.edu.pl, kabe@agh.edu.pl

Detailed information concerning manuscript preparation and review process are available at the journal's website:
www.biomaterials.pl

Subscription terms

Contact:
MSc Augustyn Powroźnik,
e-mail: apowroz@agh.edu.pl
Subscription rates:
Cost of one number: 20 PLN
Payment should be made to:
Polish Society for Biomaterials
30/A3, Mickiewicz Av.
30-059 Krakow, Poland
ING Bank Slaski S.A.
account no. 63 1050 1445 1000 0012 0085 6001

Subscription includes 4 issues and does not include special issue (conference materials).

STUDIA PODYPLOMOWE
Biomateriały – Materiały dla Medycyny
2020/2021

Organizator:	Adres:
Akademia Górniczo-Hutnicza im. Stanisława Staszica w Krakowie Wydział Inżynierii Materiałowej i Ceramiki Katedra Biomateriałów i Kompozytów **Kierownik:** prof. dr hab. inż. Elżbieta Pamuła **Sekretarz:** dr inż. Małgorzata Krok-Borkowicz	30-059 Kraków, Al. Mickiewicza 30 Pawilon A3, p. 208, 210 lub 501 tel. 12 617 44 48, 12 617 23 38, fax. 12 617 33 71 email: epamula@agh.edu.pl; krok@agh.edu.pl https://www.agh.edu.pl/ksztalcenie/oferta-ksztalcenia/ studia-podyplomowe-kursy-doksztalcajace-i-szkolenia/ biomaterialy-materialy-dla-medycyny/

Charakterystyka:

Tematyka prezentowana w trakcie zajęć obejmuje przegląd wszystkich grup materiałów dla zastosowań medycznych: metalicznych, ceramicznych, polimerowych, węglowych i kompozytowych. Słuchacze zapoznają się z metodami projektowania i wytwarzania biomateriałów a następnie możliwościami analizy ich właściwości mechanicznych, właściwości fizykochemicznych (laboratoria z metod badań: elektronowa mikroskopia skaningowa, mikroskopia sił atomowych, spektroskopia w podczerwieni, badania energii powierzchniowej i zwilżalności) i właściwości biologicznych (badania: *in vitro* i *in vivo*). Omawiane są regulacje prawne i aspekty etyczne związane z badaniami na zwierzętach i badaniami klinicznymi (norma EU ISO 10993). Słuchacze zapoznają się z najnowszymi osiągnięciami w zakresie nowoczesnych nośników leków, medycyny regeneracyjnej i inżynierii tkankowej.

Sylwetka absolwenta:

Studia adresowane są do absolwentów uczelni technicznych (inżynieria materiałowa, technologia chemiczna), przyrodniczych (chemia, biologia, biotechnologia) a także medycznych, stomatologicznych, farmaceutycznych i weterynaryjnych, pragnących zdobyć, poszerzyć i ugruntować wiedzę z zakresu inżynierii biomateriałów i nowoczesnych materiałów dla medycyny. Słuchacze zdobywają i/lub pogłębiają wiedzę z zakresu inżynierii biomateriałów. Po zakończeniu studiów wykazują się znajomością budowy, właściwości i sposobu otrzymywania materiałów przeznaczonych dla medycyny. Potrafią analizować wyniki badań i przekładać je na zachowanie się biomateriału w warunkach żywego organizmu. Ponadto słuchacze wprowadzani są w zagadnienia dotyczące wymagań normowych, etycznych i prawnych niezbędnych do wprowadzenia nowego materiału na rynek. Ukończenie studiów pozwala na nabycie umiejętności przygotowywania wniosków do Komisji Etycznych i doboru metod badawczych w zakresie analizy biozgodności materiałów.

Zasady naboru:

Termin zgłoszeń: od 20.09.2020 do 20.10.2020 (liczba miejsc ograniczona - decyduje kolejność zgłoszeń)
Wymagane dokumenty: dyplom ukończenia szkoły wyższej
Osoby przyjmujące zgłoszenia:
prof. dr hab. inż. Elżbieta Pamuła (pawilon A3, p. 208, tel. 12 617 44 48, e-mail: epamula@agh.edu.pl)
dr inż. Małgorzata Krok-Borkowicz (pawilon A3, p. 210, tel. 12 617 23 38, e-mail: krok@agh.edu.pl)

Czas trwania:	Opłaty: 2 600 zł (za dwa semestry)
2 semestry (od XI 2020 r. do VI 2021 r.) 8 zjazdów (soboty-niedziele) 1 raz w miesiącu	

ENGINEERING OF BIOMATERIALS

SPIS TREŚCI
CONTENTS

MICROSCOPIC ANALYSIS OF THE NANOSTRUCTURES IMPACT ON ENDOTHELIAL CELLS

Agnieszka Maria Kołodziejczyk[1]* ,
Magdalena Kucińska[1] , Aleksandra
Jakubowska[1] , Małgorzata Siatkowska[1] ,
Paulina Sokołowska[1,2] , Sylwia Kotarba[1] ,
Krzysztof Makowski[1,3] , Piotr Komorowski[1,3] ,
Bogdan Walkowiak[1,3]

[1] BioNanoPark Laboratories,
114/116 Dubois St., 93-465 Lodz, Poland
[2] Department of Pharmacology and Toxicology,
Medical University of Lodz,
Zeligowskiego St. 7/9, 90-752 Lodz, Poland
[3] Department of Biophysics,
Institute of Materials Science,
Lodz University of Technology,
1/15 Stefanowskiego St., 90-924 Lodz, Poland
*e-mail: a.kolodziejczyk@bionanopark.pl,
aga.szczygiel@gmail.com

Abstract

Nowadays nanostructures are more and more often designed as carriers for drug delivery, especially to improve the drug pharmacokinetics and pharmacodynamics. Numerous kinds of nanostructures are considered a good prospect for medical applications thanks to their small size, acceptable biocompatibility and toxicity. Due to the fact that nanotechnology is a new field of science, every nano-scale product must be thoroughly examined regarding its toxicity to the human body. This study provides new insights into effects of exposing endothelial cells to the selected nanostructures. Dendrimers of the fourth generation (PAMAMs), multi-walled carbon nanotubes (MWCNTs) and silver nanoparticles (SNPs) were used to evaluate nanostructures influence on endothelial cells in vitro. The nanostructures were evaluated via transmission electron microscopy and dynamic light scattering technique. The cells previously exposed to the nanostructures were observed and analyzed via the atomic force microscopy and scanning electron microscopy to obtain a quantitative evaluation of the cells morphology. The presence of multi-walled carbon nanotubes and silver nanoparticles on the cells surface was confirmed by the scanning electron microscopy. Our results confirm that the surface association and/or uptake of nanostructures by the cells resulting from physicochemical and biological processes, affect the cells morphology. Morphological changes can be induced by the membrane proteins interaction with nanomaterials, which trigger a sequence of intracellular biological processes.

Keywords: *nanostructures, atomic force microscopy, transmission electron microscopy, scanning electron microscopy, cell morphology*

Introduction

It is known that several agents (e.g. drugs, nanoparticles, cytokines) may induce changes in the cell phenotype regarding its biological and physical parameters, such as morphology, cytoskeleton reorganization, intercellular communication [1-4]. Currently, nanoparticles (NPs) are intensively studied on cells or in animal models considered as potential drug delivery or angiogenesis inhibition agents [5] thanks to their ability to improve the pharmacokinetics and pharmacodynamics of drugs. However, due to the complexity of the *in vivo* systems there are still several issues inhibiting the efficiency of NPs that need solutions to fully exploit their theoretical potential [6]. Given their small size, good biocompatibility and low toxicity, many nanoparticles are considered a promising prospect for biological and medical applications e.g. the gold [5] and the silver ones [7]. Dendrimers, due to their internal structure, can be potentially used for drug delivery, yet their metabolism by cells, tissues and organs has not been investigated enough so far [8]. Some of nanostructures, such as multi-walled carbon nanotubes (MWCNTs), are examined in nanoscience and nanotechnology for application in electronic circuits as field emitters or for hydrogen storage [9]. Still, they can be also investigated in terms of biomedical applications [10,11].

Endothelial cells (ECs) play a key role in nanomaterials delivery and their functionality. Lining the interior of the entire vascular system, ECs represent a major barrier for therapeutic agents being transferred from the bloodstream to the target tissues. One of the crucial parameters which provide information about the cells functional status, i.e. proliferation, migration or even capillary formation, are morphological changes [5].

Atomic Force Microscope (AFM) is a powerful tool to develop and assess nanoparticles [12] and characterize the properties of nanostructures [13]. Additionally, it provides nanomedicine with a versatile platform by combining the nanometer-scale resolution and the unique ability to visualize single biomolecules in their native environment [1-4] as well as nanoparticles exposed to environmental conditions. Over the last decade, AFM techniques and atomic force spectroscopy (AFS) were employed to verify the physiological state of cells [1-2], including dysfunctions after hormones, cytokines or drugs application [14-16]. An AFM probe was also postulated as a diagnostic nanosensor for cancer investigation [17-19]. Scanning electron microscopy (SEM) is yet another method to evaluate cells morphology after the nanomaterials application and to confirm the nanostructures presence on the cells membrane is [20].

The presented work studies the influence of three kinds of nanomaterials: polyamidoamine dendrimers (PAMAMs) of 4.0 generation, silver nanoparticles (SNPs) and multi-walled carbon nanotubes (MWCNTs) on the EA.hy926 endothelial cell line. The selected nanomaterials represent three main groups of nanomaterials: polymers, metals and carbon nanomaterials. The obtained results contribute to the already published works [21] on the transcriptome and proteome analysis of endothelial cells under stress conditions induced by the nanomaterials. The comprehensive analysis of the nanoparticles influence on cells morphology is vital to understand the endothelium response to drugs and other agents delivery upon the nanoparticles application.

Materials and Methods

Cell culture

The EA.hy926 endothelial cell line formed by the fusion of the HUVEC and A549 human lung carcinoma cell lines was obtained from American Type Culture Collection (ATCC® CRL-2922™) and cultured at 37°C in the humidified atmosphere of 9% CO_2 in Dulbecco's Modified Eagle Medium (DMEM, ATCC) supplemented with 10% of Fetal Bovine Serum (Gibco) and Penicillin/Streptomycin solution (ATCC). The cells were harvested for experiments before reaching 90% of confluence. Trypsin-EDTA (ATCC) was used as a dissociation solution, followed by the neutralization with the 10-fold volume of complete DMEM medium. The cells were seeded on the proper dishes for selected measurements (sterile cover glasses for AFM and SEM, cell culture dishes for TEM) and cultured for 24 h. Next, the solution of PAMAM dendrimers, SNPs or MWCNTs, in the serum-free cell culture medium was added in final concentrations, respectively (TABLE 1). The application of nanostructures at the selected concentrations caused the final toxicity of the cells - 10 and 25% [21] marked as EC 10 and EC 25.

TABLE 1. Selected concentration for AFM and SEM investigation [21].

Designation	MWCNTs [µg/ml]	SNPs [µg/ml]	PAMAM [µg/ml]
EC 10	51.7	2.8	0.07
EC 25	74.1	74.8	0.17

Dynamic light scattering

The measurements of hydrodynamic radius (R) of silver nanoparticles and dendrimers were performed using dynamic light scattering device Dyna Pro Nano Star (Wyatt). After the sonication and filtration processes (filter pores of 0.1µm), the SNPs and dendrimers suspensions in mQ water were placed in disposable cuvettes and the size distribution values (5 times with 10 acquisitions) were collected. The regularization fitting analysis to the autocorrelation functions was employed for the size calculation.

Atomic force microscopy

The atomic force microscopy was used to characterize changes in the endothelial cells morphology. The cells cultured on the cover glasses and exposed to nanostructures were fixed with a mixture solution of glutaraldehyde (2.5%) and formaldehyde (3.7%) in the phosphate buffer at pH 7.4 for 10 min. Having been fixed, the samples were rinsed with the phosphate buffer and immediately subdued to the atomic force microscopy measurements performed in a liquid chamber filled with the PBS solution. The morphology was evaluated using NTEGRA scanning probe microscope (NT-MDT, Russia) with soft cantilevers (CSG01, with the nominal spring constant 0.003 N/m and the tip radius curvature less than 10 nm, NT-MDT Probes, Russia). The scan size was 45 µm x 45 µm and the image resolution was 512 points per 512 lines.

The values of volume and surface area of the cells central part (i.e. above half of the cell height) were obtained with MountainsMap Premium 5.0 (Digital Surf) software. Additionally, the roundness parameter of the cell central part was calculated according to the formula:

$$R = Area/4\pi D^2_{max}$$

where: Area is the surface area of the apical cell part, D_{max} is the maximal diameter of the central part.

The mean value and the standard mean deviation of the morphological parameters were calculated for each experimental point (the cells exposed to the nanostructures at selected concentrations).

Additionally, the roughness parameter of 2 µm x 2 µm AFM topography scans, including the density of summits (Sds) was examined (Nova PX software). For each experimental point at least 16 images of the cells were used for calculation. The acquired data was compared with the results obtained for the control and statistical analysis of the data was performed using the variance ANOVA test to determine differences between the means for each group and the control group at the levels (*) $P<0.05$ and (**) $P<0.01$.

Scanning electron microscopy

For the scanning electron microscopy analysis, the samples were fixed for 24 h and then dehydrated with the alcohol series. Next, the samples were dried in the nitrogen stream at room temperature and a thin layer of gold (about 4 nm) was sputtered on their surface with the Leica AM ACE600 sputter.

The cell morphology was analyzed with the scanning electron microscope Quanta FEI 250 equipped with Everharta-Thornley'a (ETD) detector of secondary electrons. The microscope was working at room temperature with an accelerating voltage of 10 - 20 kV and magnification of 4000x.

Transmission electron microscopy

The silver nanoparticles and multi-walled carbon nanotubes were characterized with Transmission Electron Microscope Talos F200X (FEI) at the acceleration voltage of 200 kV working in the Scanning Transmission Electron Microscopy (STEM) and Energy Dispersive Spectroscopy (EDS) modes. The SNPs and MWCNTs were suspended in 100% ethyl alcohol and milli-Q water, respectively. After sonication, the drop of each sample was placed onto the carbon-coated copper grids (300 mesh) and dried at room temperature.

Results and Discussion

The studied nanostructures were characterized by DLS technique, TEM and EDS methods. FIG. 1 presents the results of the size distribution of PAMAM dendrimers and silver nanoparticles obtained by the DLS technique. The average value of hydrodynamic radius of PAMAM is about 1.9 nm, while for SNPs two populations of 4.3 nm and 54.9 nm are observed.

FIG. 2 presents the TEM images of SNPs where both spherical and longitudinal shapes of silver nanoparticles can be observed. The size distribution of SNPs is polydisperse, which confirms the polydispersity of SNPs observed with the DLS technique. The chemical composition of SNPs was examined with STEM (FIG. 2C) and EDS (FIG. 2D) methods. The EDS spectrum confirms a high silver content and the copper presence in the spectrum results from the use of Cu TEM grids. The other light elements are typical trace contamination.
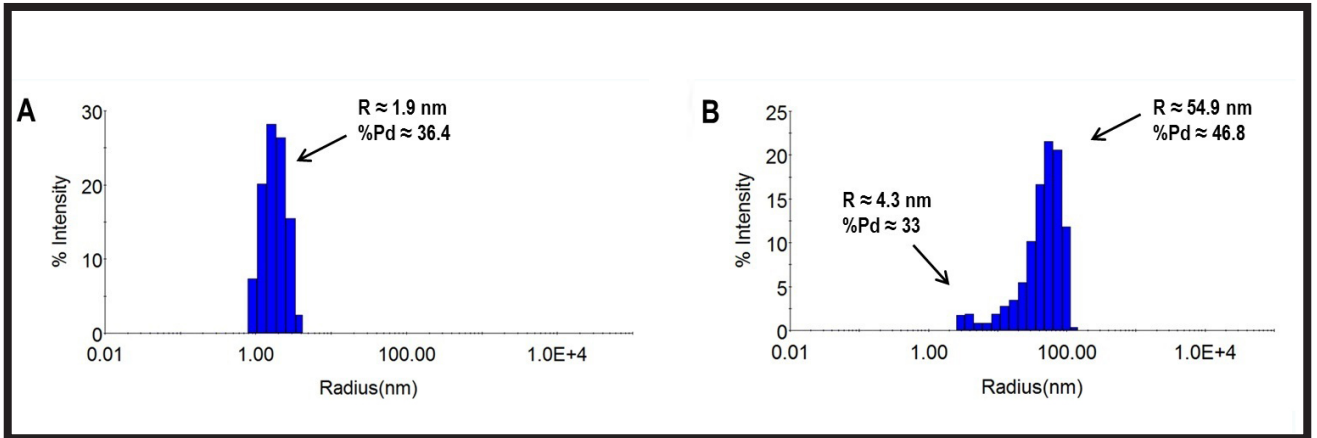
FIG. 1. Hydrodynamic radius distribution determined with DLS method in milli-Q water for PAMAMs (A) and SNPs (B). Mean value of radius (R) and % of polydispersity (%Pd) are provided.
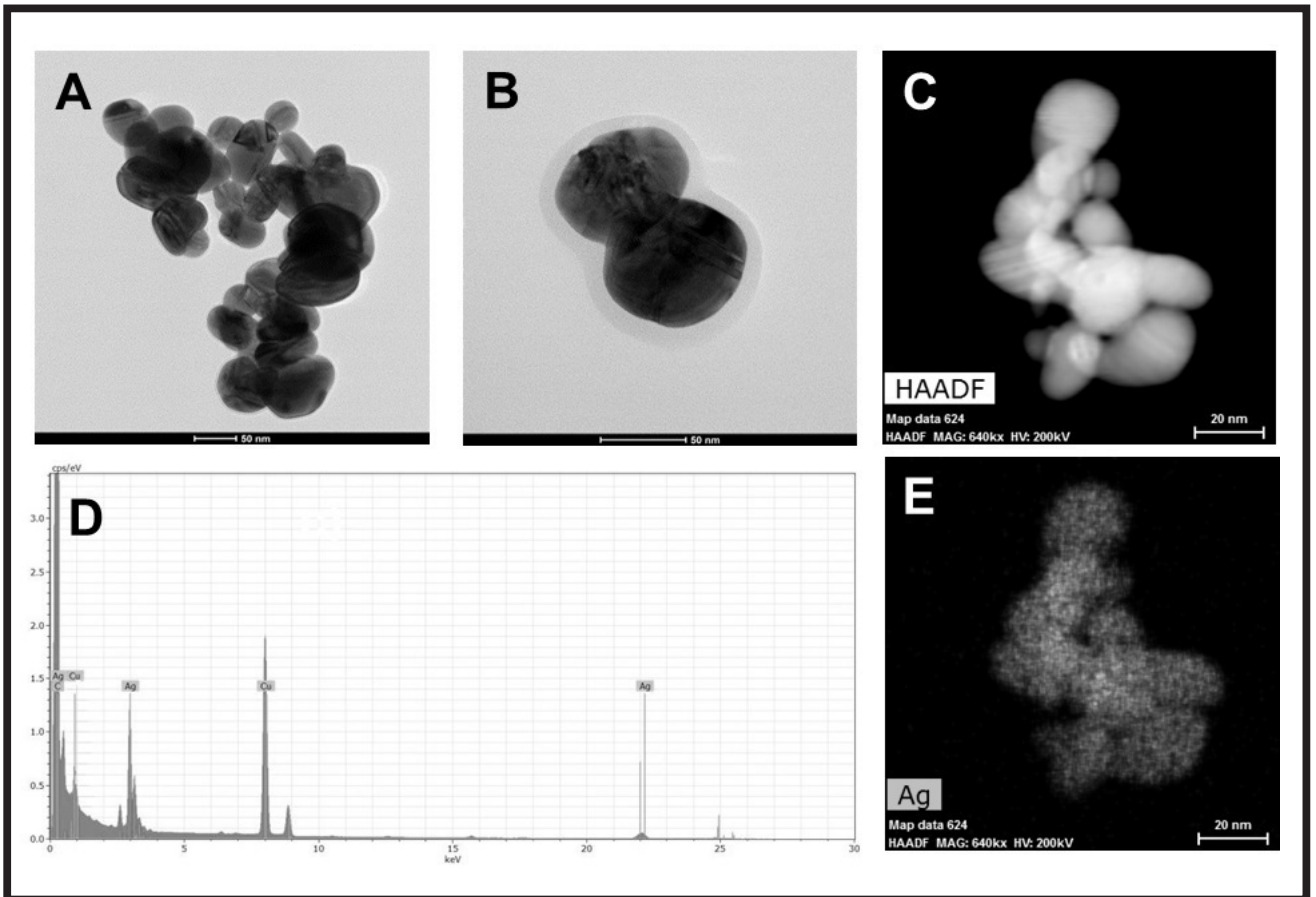

FIG. 2. TEM images of SNPs (A,B), STEM image (C), EDS spectrum (D) and EDS map of silver distribution (E).

In FIG. 3 the TEM images of MWCNTs are presented. The nanotubes are multiwalled (FIG. 3C) and the external diameter is below 20 nm. The main signal peak in the EDS spectrum (FIG. 3D) is assigned to carbon, confirming a high material purity. Copper is present in the spectrum due to the Cu TEM grids.

The cell morphology of randomly selected cells determined by the AFM method is presented in FIG. 4. The white arrows indicate agglomerates of nanostructures accumulated on the cell membrane. However, these nanostructures could also have been moved by the AFM probes while scanning the topography.

FIG. 5A presents the mean values of the surface area and the volume of the cells central parts. The statistically significant increase in the apical surface area was observed for the cells exposed to SNP or MWCNT at EC 10 and EC 25 when compared to the untreated cells (white bars, FIG. 2A). Interestingly, these nanostructures did not induce relevant changes in the cells volume (dark bars, FIG. 2A). Furthermore, the decrease in the cell roundness was observed for the cells exposed to SNP or MWCNT at EC 10 (FIG. 2B). PAMAMs dendrimers did not induce significant morphological changes at the applied concentrations.
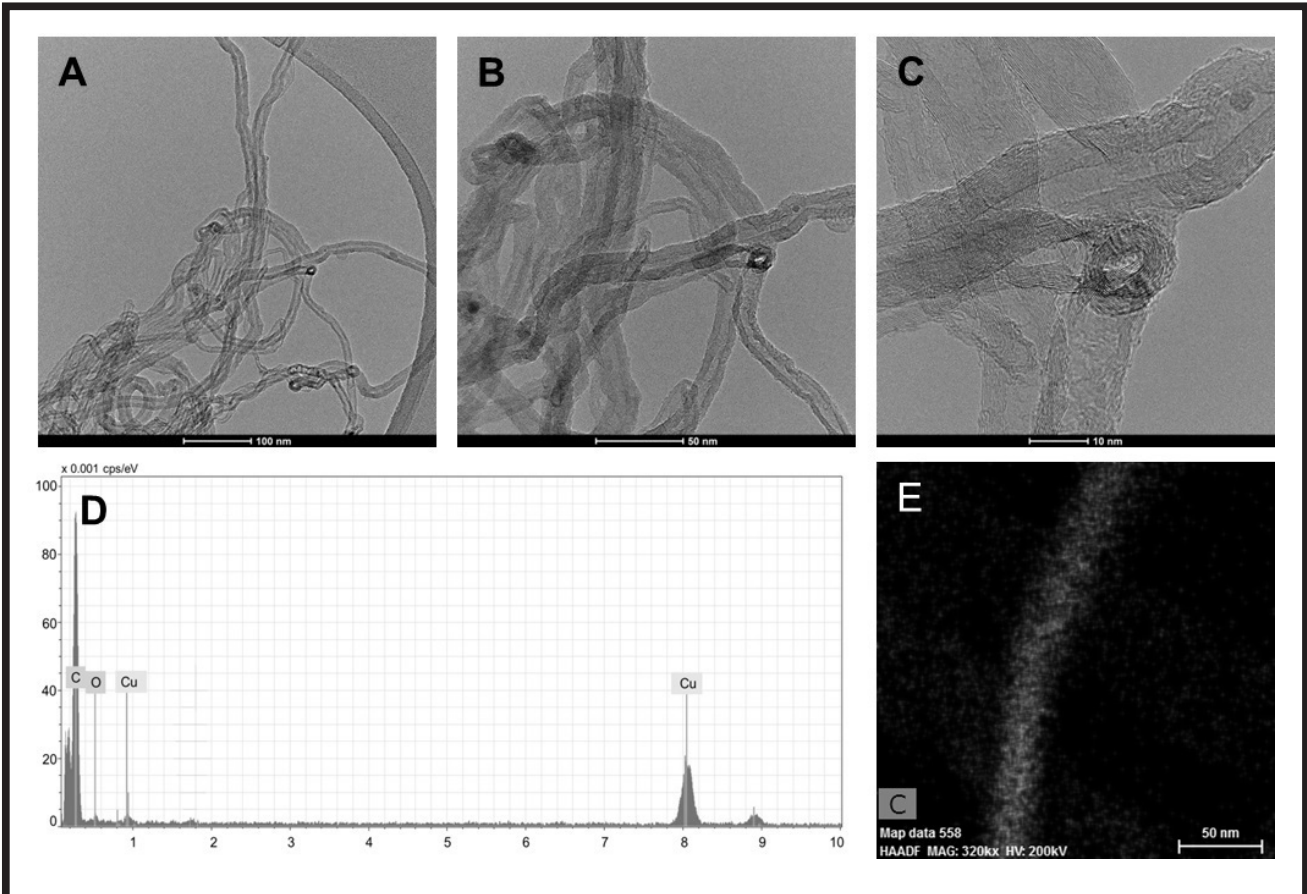
FIG. 3. TEM images of MWCNTs obtained at different magnifications: 74 000x (A), 190 000x (B), 630 000x (C), EDS spectrum (D) and EDS map of carbon distribution (E).
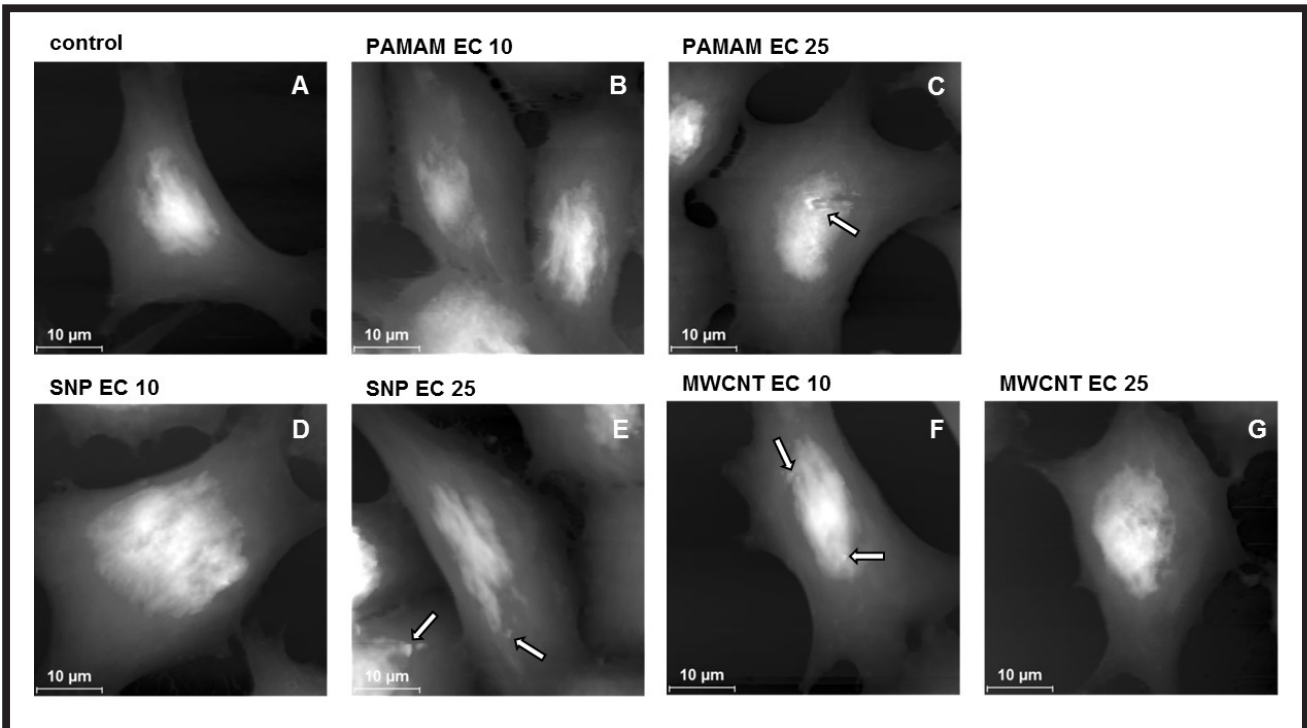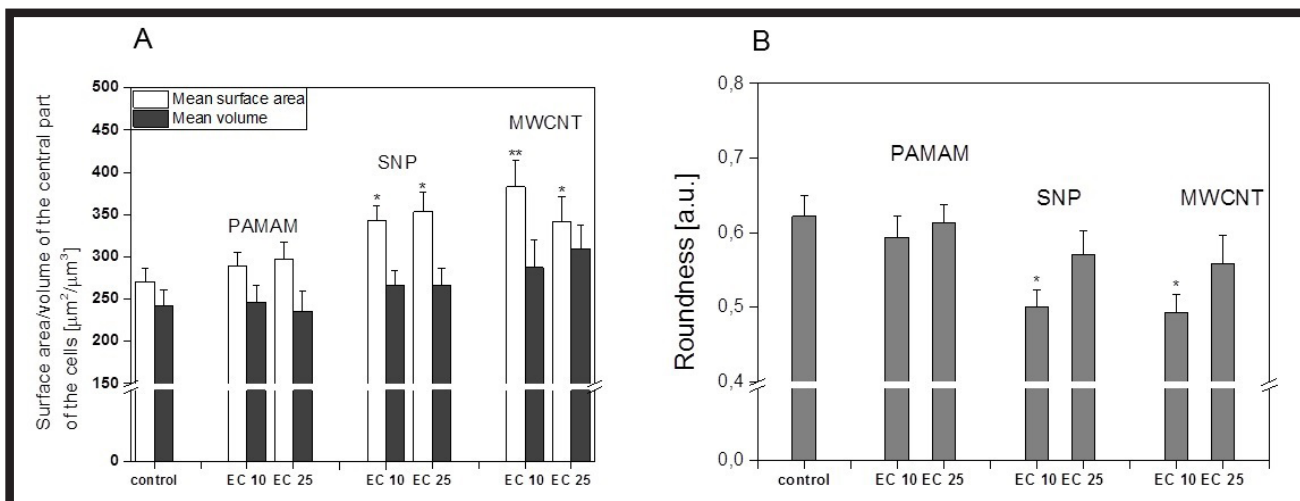

FIG. 4. AFM images (45 μm x 45 μm) of endothelial cells incubated with nanostructures. Arrows indicate agglomerates of nanostructures.

FIG. 5. Mean values of the apical volume of the cells (dark bars) and the apical surface area (white bars) (A) and mean values of the roundness of the cells (grey bars) (B). Statistically significant differences untreated cells are marked as: (*)P < 0.05 and (**)P < 0.01.

TABLE 2. Values of Sds parameter (mean ± standard mean deviation) for cells exposed to nanostructures at EC 25.

Sample	Sds [$1/\mu m^2$]
Reference	155 ± 56
PAMAM EC 25	239 ± 60
SNP EC 25	294 ± 99
MWCNT EC 25	401 ± 69 (**)

The roughness analysis (TABLE 2) indicates a significant increase in Sds value for the cells exposed to MWCNTs. This phenomenon may suggest the distinct changes in the cellular granularity related to the actin and myosin fibres reorganization and/or the nanotubes accumulation under the cell membrane.

The SEM images of the control and the cells exposed to nanoparticles at EC 10 and EC 25 are presented in FIG. 6. The huge agglomerates of MWCNTs or SNPs in the endothelial cells exposed to these nanostructures were observed (the zoom area of the attached nanostructure on the cell membrane are presented in FIGs 6 F, H).

The alterations in the sample height are visible via the AFM microscopy. However, the AFM imaging does not provide clear information about the nanomaterials localization within the cell - whether nanomaterials are on the cell surface, just below the cell membrane or inside the cell. Moreover, in some cases certain cell structures or nanomaterials and their agglomerates move along the scanning direction, that may suggest their presence on the cell surface (FIG. 4C). The AFM topography measurements were performed on the cells lacking the huge agglomerates of nanoparticles, which allowed to avoid the AFM tip damage or increase in the estimated curvature radius. For the SEM imaging, the cells with larger NMs agglomerates were selected to present the sample diversity that is necessary for cells measurements. These microscopic techniques were selected to show the effect of nanomaterials on endothelial cells in their most desirable environment. Apart from the bovine serum, cellular media contain other factors (antibiotics, L-glutamine, glucose) that can affect the agglomeration of nanostructures but maintain the cell culture in its proper conditions. It is also worth noticing that the alterations in ionic strength change the radius of dendrimers [22].

Morphological changes might be induced by the membrane proteins interaction with nanomaterials which may trigger a sequence of intracellular biological processes. Morphological changes can be linked to: the gene expression regulating cells growth and proliferation, several biological processes related to the proper protein folding, and/or cytoskeletal formation and reorganization. NPs can evoke a cytotoxic or genotoxic effect in the cell [23,24], change certain signalling pathways or alter the gene or protein expression [25].

Regarding the MWCNTs influence on mammalian cells, several papers reported that these nanomaterials lacking the surface modification were cytotoxic [26-28]. The obtained morphological results showed an increase in the apical surface area and the density of summits parameter that may be associated to the MWCNTs agglomeration, as well as the single molecules binding to the cell membrane. Similarly, when the endothelial cells were exposed to SNP at EC 10 and EC 25 concentrations, the increase in the cell surface area and the decrease in the cell roundness (at lowest concentrations) were observed. The SNPs, similarly to MWCNTs, are accumulated on the cell membrane (FIG. 6 D, E, F) and they penetrate inside, thus causing the observed changes in the cells morphology. The flow cytometry tests from our previous study confirmed the uptake of SNPs by endothelial cells which was revealed by an increase in the side (SSC) scattered light parameter [20]. In the case of the PAMAMs at EC 10 and EC 25 concentrations, there were no morphological changes as compared to the control cells.

Conclusions

The microscopic techniques can be an additional source of information characterizing the cells response to external factors present in their environment (e.g. drugs, nanomaterials). Due to the fact that nanotechnology is gaining more and more recognition in the field of medicine, every nano product should be thoroughly examined regarding its toxicity to the human body. Often, the standard methodology which includes cyto- and/or genotoxicity tests, is not sufficient and does not allow a definitive conclusion whether a given material is safe. Despite the satisfactory response of the cells in these tests, nanoparticles can exert a significant effect on the cell at the molecular level, inducing changes in the signalling pathways, expression of genes or proteins responsible for performing key functions for the cell life, which has been confirmed in numerous reports [29-32].
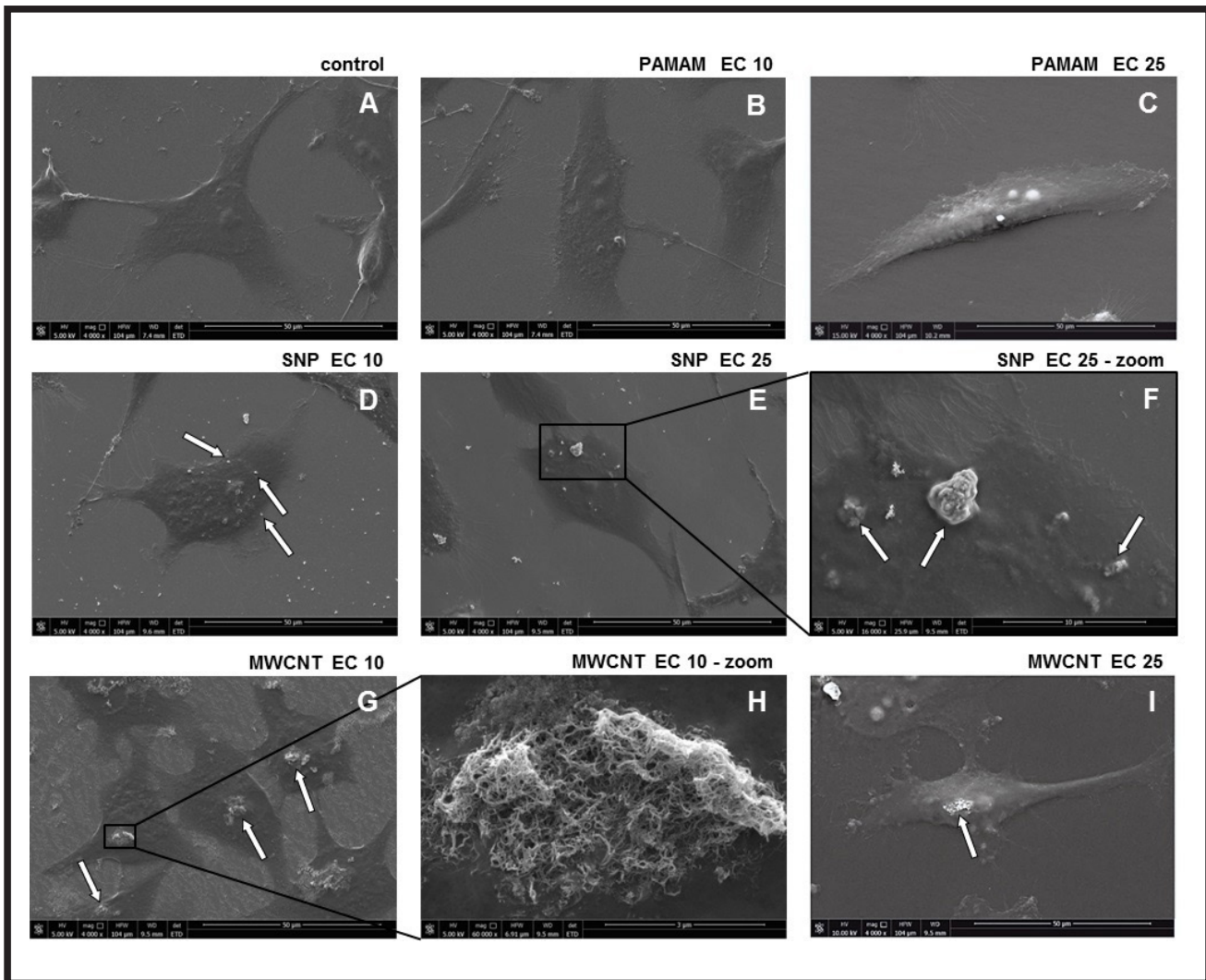
FIG. 6. SEM images of control cells (A) and cells incubated with nanostructures at EC 10 (B, D, G, H) and EC 25 (C, E, F, I). Arrows indicate examples of agglomerated nanomaterials on the cell membrane.

In our recent paper [21], it was proved that the EA.hy926 cell line after interaction with SNPs, MWCNTs and PAMAM dendrimers shows changes in the expression of numerous mRNA transcripts. Similar observations were performed while assessing the proteomic profile of these cells - the expression of proteins was significantly changed in terms of the cell growth and proliferation, apoptosis, reorganization of the cytoskeleton, synthesis of other proteins and their degradation, DNA repair, regulation of transcription, as well as the stress response.

The presented study provides new insights into evaluation of effects of exposing endothelial cells to the selected nanostructures. Both silver nanoparticles and polyhedral carbon nanotubes, used at concentrations corresponding to EC 10 and EC 25, have a significant impact on the endothelial cell morphology. Despite the widely reported toxicity of PAMAM dendrimers, our observations do not confirm such an influence of these nanostructures on endothelial cells, if used at relatively low concentrations (EC 10 and EC 25),

The microscopic techniques presented in this work may contribute to the characteristics of the cells exposed to nanomaterials, and help to establish whether the cell undergoes harmless adaptive changes, or whether the defence response to stress caused by the presence of nanomaterials in their environment begins.

ORCID iDs

A. Kolodziejczyk: https://orcid.org/0000-0003-3184-4831
M. Kucinska: https://orcid.org/0000-0003-0558-5901
A. Jakubowska: https://orcid.org/0000-0002-5531-3392
M. Siatkowska: https://orcid.org/0000-0002-4203-2567
P. Sokolowska: https://orcid.org/0000-0002-6290-7172
S. Kotarba: https://orcid.org/0000-0003-1490-0627
K. Makowski: https://orcid.org/0000-0002-7885-3420
P. Komorowski: https://orcid.org/0000-0002-4035-7501
B. Walkowiak: https://orcid.org/0000-0003-4867-5456

References

[1] A.M. Szczygiel, G. Brzezinka, M. Targosz-Korecka, S. Chlopicki, M. Szymonski: Elasticity changes anti-correlate with NO production for human endothelial cells stimulated with TNF-α. Pflugers Archiv: European journal of physiology 463(3) (2011) 487-496.

[2] A.M. Kolodziejczyk, G.D. Brzezinka, K. Khurana, M. Targosz-Korecka, M. Szymonski: Nanomechanical sensing of the endothelial cell response to anti-inflammatory action of 1-methylnicotinamide chloride. Int. J. Nanomedicine 8 (2013) 2757-2767.

[3] T. Wojcik, E. Buczek, K. Majzner, A. Kolodziejczyk, J. Miszczyk, P. Kaczara, W. Kwiatek, M. Baranska, M. Szymonski, S. Chlopicki: Comparative endothelial profiling of doxorubicin and daunorubicin in cultured endothelial cells. Toxicology In Vitro 29(3) (2015) 512-521.

[4] M. Targosz-Korecka, R. Biedron, A.M. Szczygiel, G. Brzezinka, J. Szczerbinski, A. Zuk: Stiffness changes of tumor HEp2 cells correlates with the inhibition and release of TRAIL-induced apoptosis pathways. J. Mol. Recognit. 25 (2012) 299-308.

[5] Y. Pan, Q. Wu, L. Qin, J. Cai, B. Du: Gold Nanoparticles Inhibit VEGF165-Induced Migration and Tube Formation of Endothelial Cells via the Akt Pathway. BioMed Research International 2014 (2014) 1-11.

[6] S.P. Samuel, N. Jain, F. O'Dowd, T. Paul, D. Kashanin, V.A. Gerard, Y.K. Gunko, A. Prina-Mello, Y. Volkov: Multifactorial determinants that govern nanoparticle uptake by human endothelial cells under flow. Int. J. Nanomedicine 7 (2012) 2943-2956.

[7] Nanomaterials (Basel). 2018 Aug 31;8(9). pii: E681. doi: 10.3390/nano8090681. Biomedical Applications of Silver Nanoparticles: An Up-to-Date Overview

[8] S. Sekowski, K. Milowska, T. Gabryelak: Dendrimers in biomedical sciences and nanotechnology. Postepy Hig. Med. Dosw. 62 (2008) 725-733.

[9] A. Bachmatiuk: Badania nad technologią otrzymywania i właściwościami nanorurek węglowych, Szczecin, 2008

[10] S. Beg, M. Rizwan, A.M. Sheikh, M.S. Hasnain, K. Anwer, K. Kohli: Advancement in carbon nanotubes: basics, biomedical applications and toxicity. Journal of Pharmacy and Pharmacology 63 (2011) 141-163.

[11] A.C.A. Wan, J.Y. Ying: Nanomaterials for in situ cell delivery and tissue regeneration. Advanced Drug Delivery Reviews 62 (2010) 731-740.

[12] S. Schiwek, L. Heim, R.W. Stark, C. Dietz: Manipulation of polystyrene nanoparticles on a silicon wafer in the peak force tapping mode in water: pH-dependent friction and adhesion force. Journal of Applied Physics 117 (2015) 104303.

[13] K. Safarova, A. Dvorak, R. Kubinek, M. Vujtek, A. Rek: Usage of AFM, SEM and TEM for the research of carbon nanotubes, in: A. Mendez-Vilas, J. Diaz (Eds), Modern Research and Educational Topics in Microscopy, Formatex (2007) 513-519.

[14] H. Oberleithner, C. Riethmullera, H. Schillersa, A.M.G. Graham, H.E. de Wardener, M. Hausberg: Plasma sodium stiffens vascular endothelium and reduces nitric oxide release. PNAS 104(41) (2007) 16281-16286.

[15] H. Oberleithner, C. Riethmuller, T. Ludwig, M. Hausberg, H. Schillers: Aldosterone remodels human endothelium. Acta Physiol 187 (2006) 305-312.

[16] H. Oberleithner, C. Callies, K. Kusche-Vihrog, H. Schillers, V. Shahin, C. Riethmüller: Potassium softens vascular endothelium and increases nitric oxide release. Proc. Natl. Acad. Sci. USA 106(8) (2009) 2829-2834.

[17] M. Lekka: Atomic force microscopy: A tip for diagnosing cancer. Nature Nanotechnology 7 (2012) 691-692.

[18] M. Lekka, P. Laidler, D. Gil, J. Lekki, Z. Stachura, A.Z. Hrynkiewicz: Elasticity of normal and cancerous human bladder cells studied by scanning force microscopy. Eur Biophys J 28 (1999) 312-316.

[19] M. Plodinec, M. Loparic, C.A. Monnier, E.C. Obermann, R. Zanetti-Dallenbach, P. Oertle, et al.: The nanomechanical signature of breast cancer. Nature Nanotechnology 7 (2012) 757-765.

[20] P. Sokołowska, K. Białkowska, M. Siatkowska, M. Rosowski, M. Kucińska, P. Komorowski et al.: Human brain endothelial barrier cells are distinctly less vulnerable to silver nanoparticles toxicity than human blood vessel cells. Nanomedicine: Nanotechnology, Biology and Medicine 13(7) (2017) 2127-2130.

[21] P. Komorowski, M. Siatkowska, T. Wasiak, K. Działoszynska, S. Kotarba, K. Kądzioła et al.: Simultaneous transcriptome and proteome analysis of EA.hy926 cells under stress conditions induced by nanomaterials. J Biomed Mater Res B Part B. 000B (2018) 1-11

[22] P.K. Maiti, T. Cagin, S.T. Lin, W.A. Goddard: Effect of Solvent and pH on the Structure of PAMAM Dendrimers. Macromolecules 38 (2005) 979-991.

[23] L. Shang, K. Nienhaus, G.U. Nienhaus: Engineered nanoparticles interacting with cells: size matters. Journal of Nanobiotechnology 12 (2014) 1-11.

[24] K. Savolainen, H. Alenius, H. Norppa, L. Pylkkänen, T. Tuomi, G. Kasper: Risk assessment of engineered nanomaterials and nanotechnologies - A review. Toxicology 269 (2010) 92-104.

[25] E. Bajak, M. Fabbri, J. Ponti, S. Gioria, I. Ojea-Jimenez, A. Collotta, V. Mariani, D. Gilliland, F. Rossi, L. Gribaldo: Changes in Caco-2 cells transcriptome profiles upon exposure to gold nanoparticles. Toxicology Letters 233 (2015) 187-199.

[26] S. Hirano, S. Kanno, A. Furuyama: Multi-walled carbon nanotubes injure the plasma membrane of macrophages. Toxicol. Appl. Pharmacol. 232 (2008) 244-251.

[27] C. Cheng, K.H. Muller, K.K.K. Koziol, J.N. Skepper, P.A. Midgley, M.E. Welland, A.E. Porter: Toxicity and imaging of multi-walled carbon nanotubes in human macrophage cells. Biomaterials 30 (2009) 4152-4160.

[28] X. Chen, H.J. Schluesener: Multi-walled carbon nanotubes affect drug transport across cell membrane in rat astrocytes. Nanotechnology 21 (2010) 105104.

[29] S.C. Tilton, N.J. Karin, A. Tolic, Y. Xie, X. Lai, R.F.Jr. Hamilton, K.M. Waters, A. Holian, F.A. Witzmann, G. Orr: Three human cell types respond to multi-walled carbon nanotubes and titanium dioxide nanobelts with cell-specific transcriptomic and proteomic expression patterns. Nanotoxicology 8(5) (2014) 533-548.

[30] M. Marmiroli, D. Imperiale, L. Pagano, M. Villani, A. Zappettini, N. Marmiroli: The Proteomic Response of Arabidopsis thaliana to Cadmium Sulfide Quantum Dots, and Its Correlation with the Transcriptomic Response. Front Plant Sci. 6 (2015) 1104.

[31] L. Chen, X. Meng, J. Gu, W. Fan, N. Abdlli, F.A. Peprah, N. Wang, F. Zhu, P. Lü, S.Ma, K. Chen: Silver nanoparticle toxicity in silkworms: Omics technologies for a mechanistic understanding. Ecotoxicol Environ Saf. 172 (2019) 388-395.

[32] S. Gioria, P. Urbán, M. Hajduch, P. Barboro, N. Cabaleiro, R. La Spina, H. Chassaigne: Proteomics study of silver nanoparticles on Caco-2 cells. Toxicol In Vitro 50 (2018) 347-372.

THE EFFECT OF HYDROXYAPATITE COATING WITH SILVER NANOPARTICLES ON OSSEOINTEGRATION OF TITANIUM IMPLANTS

Joanna Sulej-Chojnacka[1]* , Waldemar Woźniak[2] , Daniel Andrzejewski[1]

[1] Lukasiewicz Research Network - Metal Forming Institute,
14 Jana Pawla II St., 61-139 Poznan, Poland
[2] Wiktor Degi Orthopedic and Rehabilitation Clinical Hospital, Karol Marcinkowski Medical University, Department of General Orthopedics, Oncology and Traumatology,
135-147 28 Czerwca 1956 r. St., 61-545 Poznan, Poland
*e-mail: joanna.chojnacka@inop.poznan.pl

Abstract

During the implantation surgery, an infection associated with the biofilm formation may occur. Both the type of the introduced material as well as the implant osseointegration largely determine the effectiveness of bone defect treatment. The materials research is increasingly focusing on improving the osseointegration process. A bacterial biofilm can form on any surface of the artificial organ that has been introduced into the body or surrounding tissues. A bacterial infection is one of the most serious complications of implantology surgery leading to serious physiological damage. As proved in the literature, a solution that can prevent bacterial infections is to modify the implant surface by applying an antibacterial coating, while maintaining the material biocompatibility. The article presents the tests results of prototype implants with hydroxyapatite coatings obtained via plasma spraying on titanium surfaces. The resulting coatings were enriched with silver nanoparticles, the content of which was about 2%. The animal model are New Zealand rabbits. The implants were placed in the femur of the animal. The amount of released ions and the force of pulling the implants from the bone were determined. The binding strength between the joint surface and the implant was determined by the mechanical blocking and biological binding of growing bone tissue. In addition, the surface structure of the obtained implants was evaluated.

It has been shown that the surface modification of the implants affected the obtained stabilization value, as compared to the implants surface coated only with hydroxyapatite.

Keywords: implant, hydroxyapatite, Ti6Al4V, silver nanoparticles

Introduction

Hip arthroplasty is one of the most commonly performed surgical procedures consisting in the complete replacement of a damaged joint by an artificial one. Such surgery is connected with introducing foreign bodies into the human internal environment with the assumption that they will meet the long-term biomechanical function and are biologically inert [1]. The effectiveness of bone loss treatment predominantly depends on the implant osseointegration [2] and the proper selection of the implant material, which can eliminate possible complications in orthopedic surgery [2].

In order to develop implantology by improving osseointegration the implant surface may be modified in several aspects, such as topography, surface chemistry, and physical surface properties (surface charge and energy) [3]. The osseointegration process ("direct structural and functional connection between the bone and the surface of the loaded implant") is a decisive factor in the success of endoprosthesis implant surgery. The binding strength between the joint and the implant is determined by the mechanical blocking and biological binding of growing bone tissue. Implants with rough surfaces or porous coatings provide excellent mechanical coupling with the surrounding bone and achieve greater stability [4,5].

Alloplastic materials, e.g. titanium, can induce different defense reactions, including implant rejection. The material is considered biocompatible when it does not cause pathological reactions in the tissues, does not emit any disintegrating substances, and - in the case of implants - it allows the bone to grow directly on the intraosseous surface [5]. One of the biocompatible materials widely used in medicine is titanium and its alloys. As the binding strength between the bone tissue and the biological surface of a titanium-based alloy is weak [6], many studies have been carried out to improve the osseointegration of titanium and the bone-implant binding. Particular attention has been paid to the combination of surface modification and applying bioactive coatings on titanium-based alloy surfaces. To strengthen the bioactivity of implant metal surfaces, hydroxyapatite (HA) is often used as a thin coating [7,8]. Unfortunately, the excellent biocompatibility of HA also allows the adhesion and reproduction of bacteria on the surface, which leads to the infection and the possible implant rejection. A bacterial infection is one of the most serious implant surgery complications that may lead to severe physical damage and the need for additional costly surgical procedures. Therefore, the incorporation of anti-bacterial components into the hydroxyapatite coating during or after the production process is of great clinical significance. An inorganic antibacterial material containing silver, copper, zinc and other metal ions has excellent properties, such as thermal stability and broad spectral antimicrobial properties. Of all the antimicrobial metal ions, silver ions not only have the best antibacterial activity including gram-positive, gram-negative bacteria, fungi and even viruses [9], but also the lowest cytotoxicity [7,10]. In contrast to the bactericidal action of silver ions, the antibacterial activity of colloidal silver particles depends on their size. The smaller the particles, the greater the antibacterial effect [11]. When nanoparticles (Np) are used, there is a huge increase in the contact surface with microbial cells and the prolonged antibacterial action is associated with a gradual release of ions from the implant surface in a process lasting up to several months [12]. Silver-based composite implants require not only sufficient bactericidal properties but also the extended and controlled release of silver from the material.

The monitored release of silver ions inhibits bacterial proliferation. The authors of [13] showed that the amount of released silver ions depends on the immersion time and the amount of nanoparticles incorporated into the polymer matrix. During the incubation, the release of silver ions increases in proportion to the square root of the fill content. Due to the polymer stability in the composite, the release does not proceed rapidly. In addition, it was proved that silver does not affect the pH of the solution of any of the tested composites, hence the tested materials are safe for bones and the surrounding tissues. The composites with higher nano addition content were more hydrophobic and had a greater roughness. What is more, as the roughness increases, the amount of released silver ions increases, and the better bactericidal efficacy is observed [13,14].

In the presented studies, powdered hydroxyapatite was sprayed onto the surface of cylindrical titanium samples (implants), then silver nanoparticles were deposited and the prototypes of the implants obtained in this way were tested for ion release during time and bone hyperplasia. The presented work examined the strength of extraction of implants from bones. The influence of nano additive on the osseointegrative properties of hydroxyapatite coatings was analyzed. For comparison, HA coated implant was used.

Materials and Methods

Production of implants with HA and HA+AgNp coatings

Titanium and titanium alloys, especially Ti6Al4V are the most attractive biocompatible alloys due to their excellent combination of mechanical properties, corrosion resistance and biocompatibility. For this reason, a titanium alloy was used as a research material. The prototype implants were made of titanium alloy Ti6Al4V (the material was obtained from 2PS Company, Montbazens Germany) coated with hydroxyapatite and with hydroxyapatite with silver nanoparticles. The titanium samples measuring 4 mm in diameter and 10 mm in length were coated with HA by the plasma spraying method in the French company 2PS. The plasma spraying was used as a traditional technique preferred by industrialists due to its moderate costs, ease of implementation and high efficiency. In addition, plasma spraying is used to produce almost all commercially available HAP coatings for orthopedic and dental implants. Schematic diagrams of the prototype implants are presented in FIG. 1. Next, the process of applying silver nanoparticles on the samples with the HA coating was carried out on a specially prepared stand (FIG. 2).
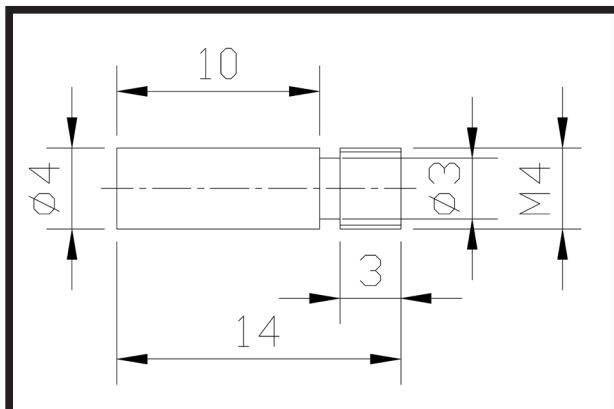

FIG. 1. Diagram of Ti6Al4V prototype implant.

The in vivo samples were fixed in a specially made holder (FIG. 2). The process of mixing the suspension was carried out at the speed of 600 rpm, using an aqueous suspension of silver particles manufactured by *Particular* GmbH (Hannover Germany) with a particle size of 66 nm and a concentration of 106 mg/l. The samples were then dried in a laboratory furnace at 70°C for 1 h.

Microscopic observations

Microscopic observations of the surface morphology of the prototype implants were conducted using an Inspect S scanning electron microscope (FEI). The amount of silver nanoparticles on the surface of the implants was monitored by SEM-EDS.
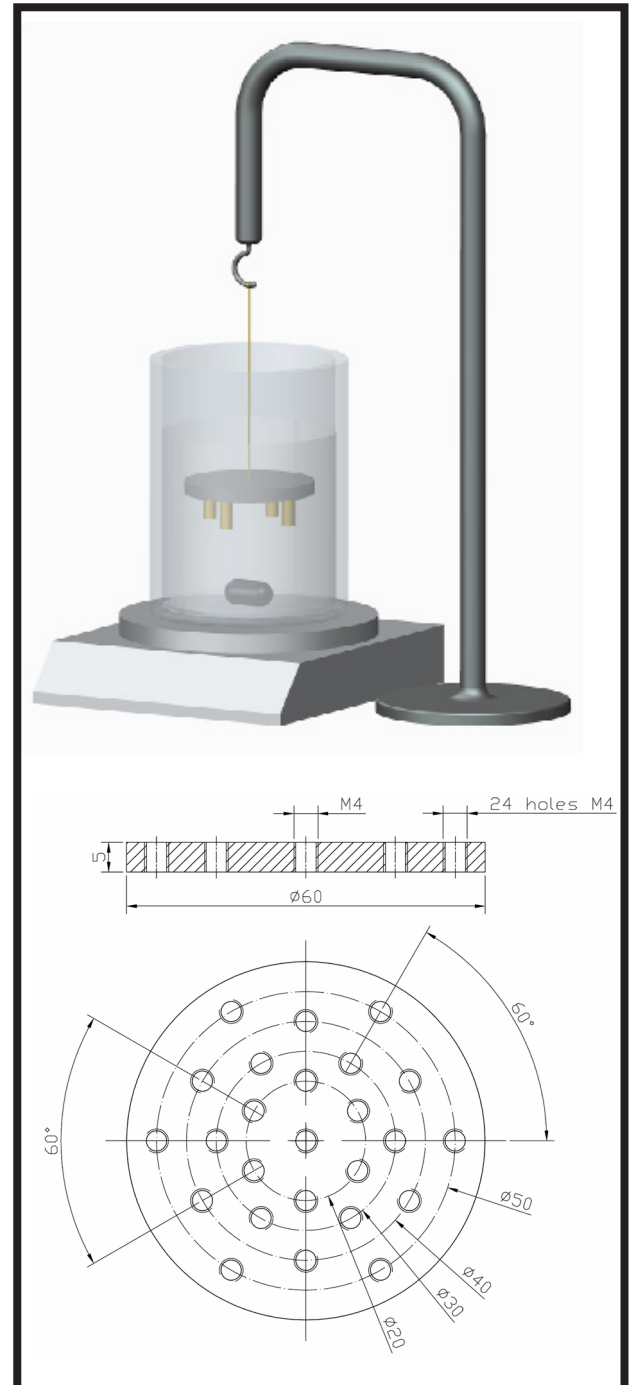

FIG. 2. Diagram of silver nanoparticle application stand and in vivo sample fixing.

Ion release studies

The first batch of the prototype implants was subjected to the ion release testing. The samples were placed with 100 ml of ultrapure water in four flat-bottomed sealed flasks. The content of silver ions was analyzed after removing the sample from the relevant flask after 12 h, 7, 14 and 21 days. The experiment was repeated three times for each period and the presented results are the average of the measurements. In addition, the ion conductivity test was performed for each of the obtained samples. The measurement was carried out at room temperature, the reference sample was ultrapure water with a conductivity of 1.28 µS/cm. Additionally, the analysis of the silver ions concentration was performed. The elements were determined by atomic absorption spectrometry with atomization in a graphite cuvette using a Varian Spectra AA 200 apparatus. The atomic absorption method with atomization in a graphite cuvette is a sensitive method useful for trace metal analysis.

In vivo studies

In vivo studies were conducted on a group of 10 New Zealand rabbits weighing between 2.3 and 3.7 kg. The animals underwent implant surgeries. Five rabbits received the implants with the hydroxyapatite coating, and the other five ones - the implants with the hydroxyapatite coating enriched with silver nanoparticles. Having immobilized the rabbit, the joint was exposed. The hair was shaved and the skin was disinfected with alcohol and iodine and prepared for the sterile operation. Then a lateral parapatellar skin incision was made extending from a level at about 1.5 cm above the patella to the tibial tuberosity. The subcutaneous tissue was incised in the same line. Then a similar curved incision was made in the fascia lata and lateral fascia of the stifle joint. Enough fascia was left on the lateral border of the patella to receive enough space for sutures when the joint is closed. After opening a joint capsule, the patella was luxated medially and the femoral trochlea was exposed. With the knee maximally flexed a full-thickness cylindrical defect was created (5 mm in diameter) at the bottom of the trochlear groove, parallel to the cortical bone, using a drill-bit and a trephine. Firstly, the predrilling was performed using a drill-bit smaller diameter and the defect was gradually enlarged to the level of 5 mm. All debris was removed and the area was flushed with saline solution. Then the titanium implant was inserted. Five rabbits received implants with initial HAP and the rest of them – the same implants but modified with AgNps. The implants were fitted at the sub-chondral bone level, beneath the surface of the adjacent articular cartilage to ensure a good connection with the bone marrow. Subsequently, the patella was repositioned and the joint capsule closed with a continuous suture pattern using Dexon 3-0. Then the fascia, subcutaneous tissue and the skin were closed in the routine manner with absorbable suture material. After the operation, all the rabbits were allowed to move freely in the cages without any splints.

To minimize the risk of post-operative infection, the animals were given an antibiotic and an anti-inflammatory drug for 5 days after the surgery. After a 2-month observation period, the animals were euthanized (blood, kidney and liver tissue samples were collected for further evaluation). A fragment of the thigh bone together with the implant was removed from each rabbit and fixed in a paraformaldehyde buffer solution with a pH of 7.4. All the implantation activities were carried out with the consent of the Ethics Committee for Experiments on Animals. All the tests were performed by the Poznan University of Medical Sciences (UMP) scientists holding proper permissions for research from the Local Bioethics Commission for Research on Animals in Poznan.

Measurements of the force of removing implants from bone

Assessment of the force used to remove the implant from the bone is a method used to evaluate the implant stability. The test is based on measuring the tensile force at which the implant is extracted from the bone - the higher the measured value, the better implant stabilization. The method also indirectly provides information on the implant stabilization in the bone.

In order to measure the force of extracting the implants from the bone, a special holder for fixing the sample was designed at the Lukasiewicz Research Network-Metal Forming Institute in Poznan. FIG. 3 shows the scheme of fixing the sample in the holder to perform a static tensile test.

The measurements were carried out using a testing machine - Instron 4483 series H1907 with a 2518-102 measuring head with a lifting capacity of 20 kN and a 500-181-20 electronic caliper (Mitutoyo). The tests were carried out at 21.5°C. The maximum force value was noted as the force needed to extract the implant from the bone. FIG. 4 shows an example of the sample, i.e. the bone fragment with the implant.
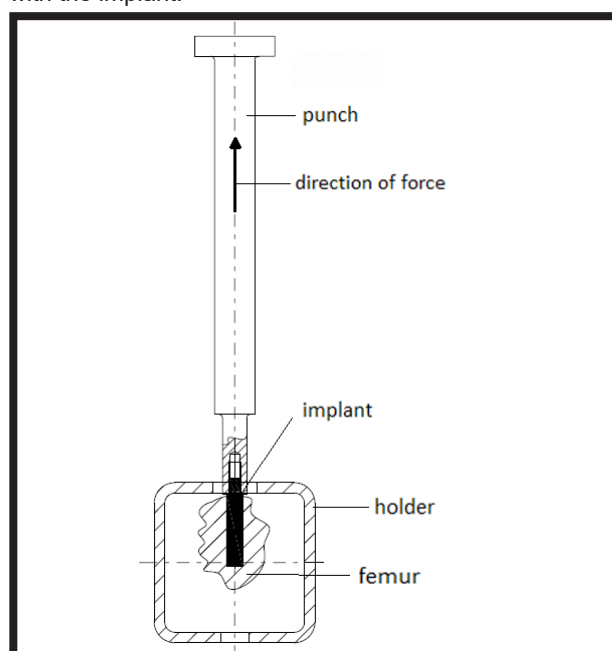

FIG. 3. Diagram of the sample fixing.

FIG. 4. The example of the in vivo sample.

Results and Discussion

The microscopic analysis of the prototype implant surface was performed. FIG. 5 shows the SEM micrographs of the hydroxyapatite coating obtained under conditions typical of the industrial process. The HA coating is characterized by low porosity and the presence of microcracks. Irregularities resulting from imperfections in the machining process are also visible. In industry the presence of several microcracks is acceptable. The spherical HA particles of a smaller size than the initial particles are also visible in the SEM micrographs. The reduction in HA grain size results from the partial melting and evaporation in the plasma stream.

The SEM micrographs of the hydroxyapatite surface after the silver nanoparticle application process are shown in FIG. 6; the arrows indicate the nAg particles occurring on the surface. The distribution of silver nanoparticles on the implant surface was virtually uniform. In addition, no significant agglomerates were observed, only those that occur sporadically. The elemental composition analysis showed the presence of Ag nanoparticles at the level of 2%. The results of EDS analysis are presented in FIG. 7.
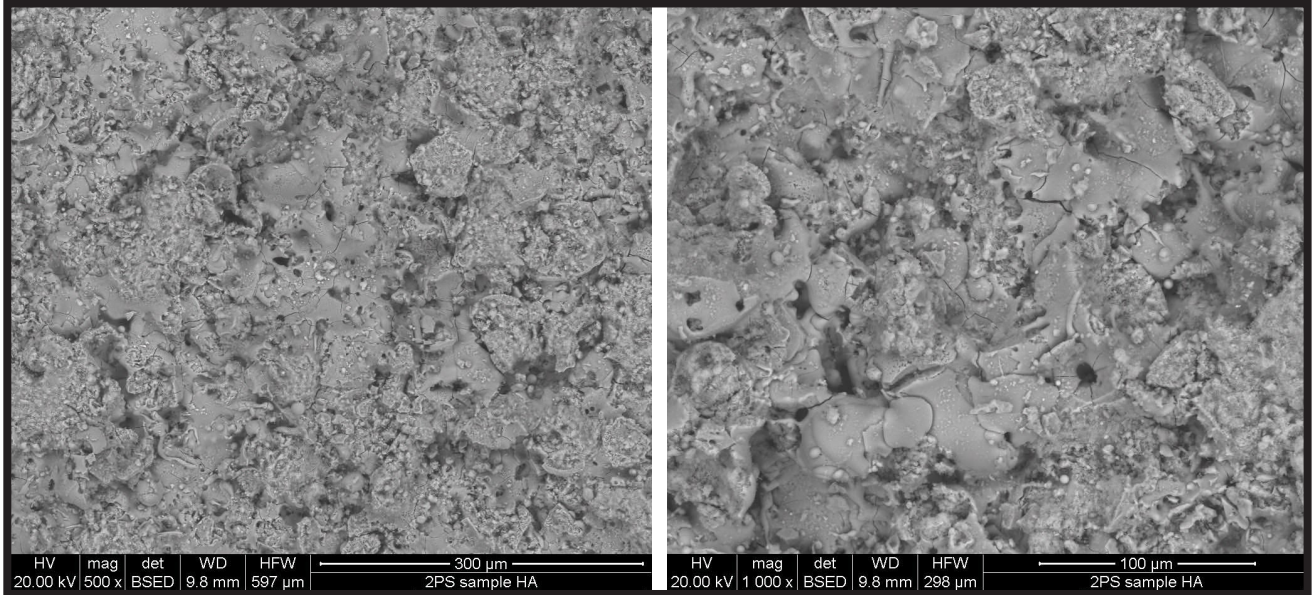

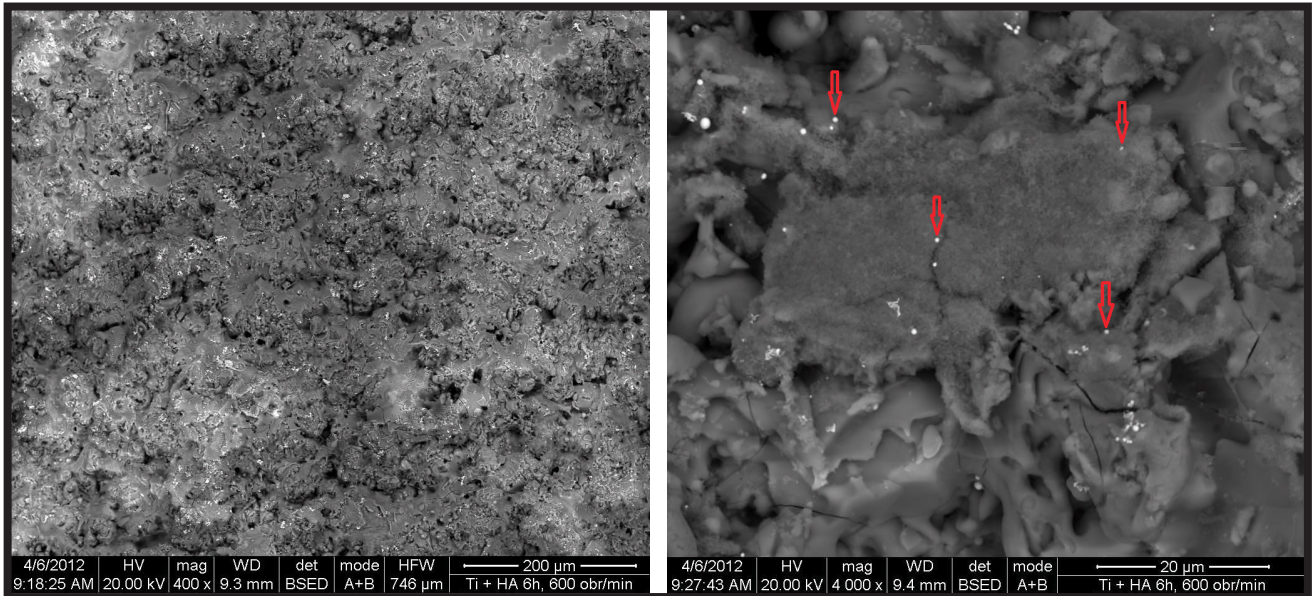**FIG. 5. SEM micrographs of hydroxyapatite coating applied on Ti6Al4V.**

FIG. 6. SEM micrographs of hydroxyapatite coating with silver nanoparticles on the surface of Ti6Al4V, with different magnification.
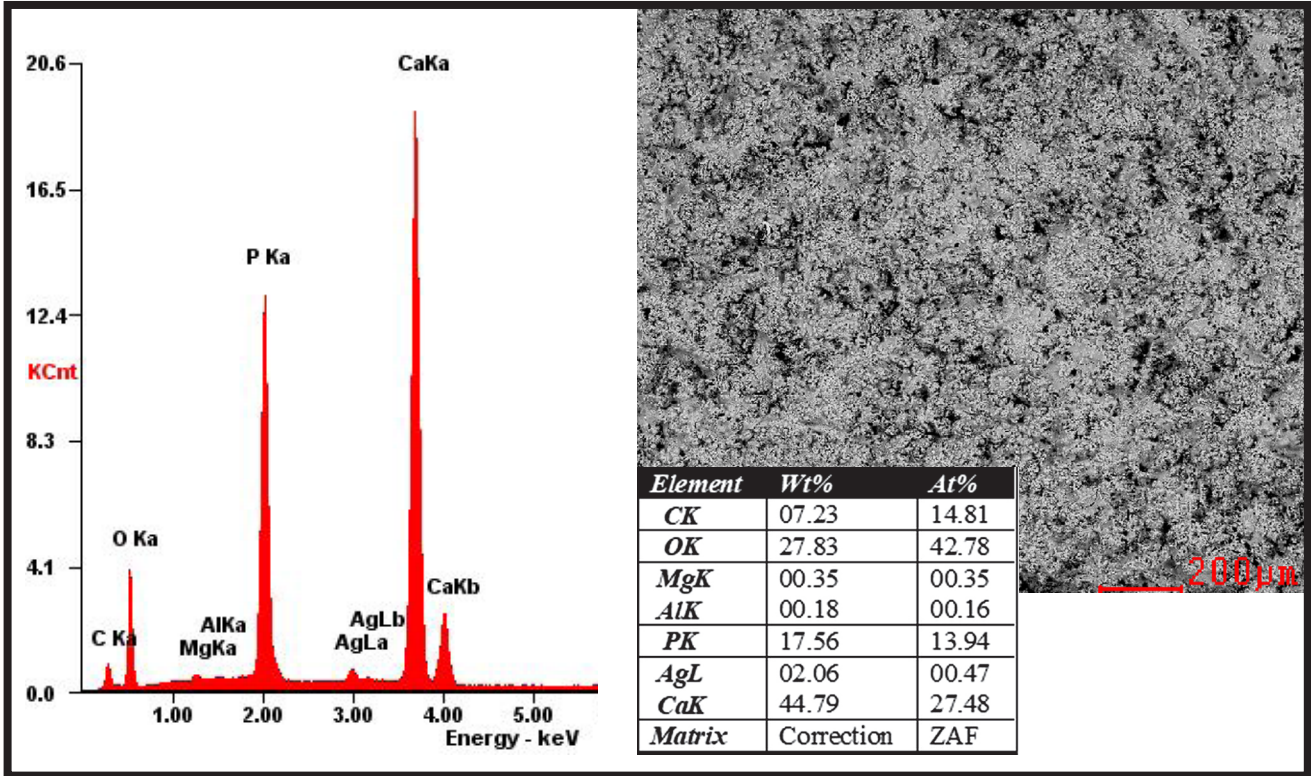
FIG. 7. Elemental composition analysis of the coating.

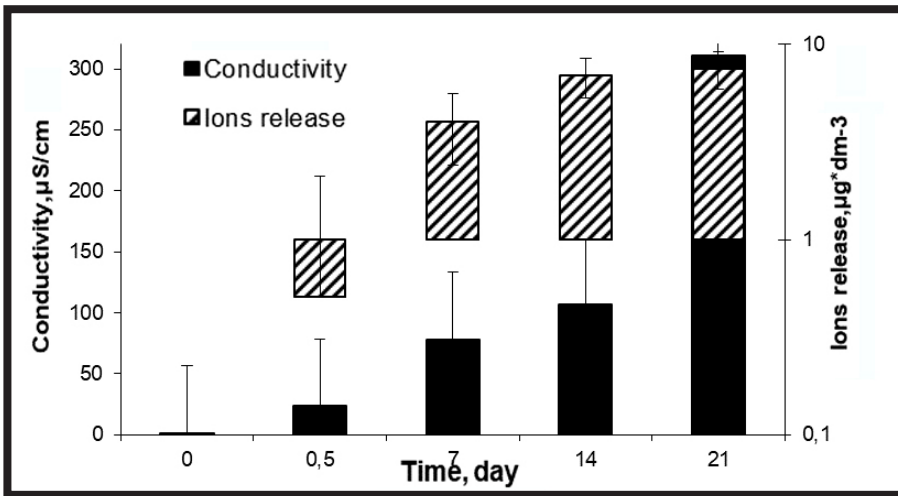| Element	Wt%	At%
CK	07.23	14.81
OK	27.83	42.78
MgK	00.35	00.35
AlK	00.18	00.16
PK	17.56	13.94
AgL	02.06	00.47
CaK	44.79	27.48
Matrix	Correction	ZAF

FIG. 8. Ion conductivity as a function of incubation time.

In addition, the ion conductivity test was carried out for the obtained prototypes. The measurement was performed at room temperature, and the reference sample was ultrapure water with a conductivity of 1.28 µS/cm (time equal to 0). The dependence of the ionic conductivity on time and the dependence of silver ion content on the incubation time are shown in FIG. 8.

The analysis of the data presented in FIG. 8 allowed the authors to conclude that with the longer the incubation time of the implants with the HA+AgNp coating, the higher the ionic conductivity and the content of released silver ions. After 21 days, the conductivity of the solution reached the value of 311 µS/cm and the concentration of silver ions was 7.54 µg·dm^{-3}. This proved that over time an increasing number of ions got released into the solution, including silver ions when keeping the tested material in ultrapure water. During the first 7 days, there was an increase in the concentration of silver ions to the level of 3.52 µg·dm^{-3}, in the following 7 days the concentration increased by 2.89 µg·dm^{-3} and in the last week - by 1.32 µg·dm^{-3}.

During the test, however, no changes in the pH value were observed, i.e. the acid-base balance of the liquid was not disturbed. For this reason, it may be assumed that the material is safe for adjacent bones and tissues of the human body. Similar results were obtained by the authors of the work [13].

Measurements of the implant stability in bone in animal models can be used to assess the degree and quality of osseointegration. Bone remodeling is a lifelong process, the alternating occurrence of bone resorption and new bone formation. In the peri-implant area, the remodeling process is distinctly observed after 6-12 weeks after the surgical implantation [15]. The in vivo tests confirmed that the prototypes of the Ti6Al4V+HA and Ti6Al4V+HA+AgNp implants exhibited good surgical functionality and remained in the place of implantation. After the operation, all the animals moved freely in their cages, the majority of rabbits had mild swelling around the suture but they did not stumble. After two weeks, all the operated animals were in good general condition, with no clinical signs of dysfunction.
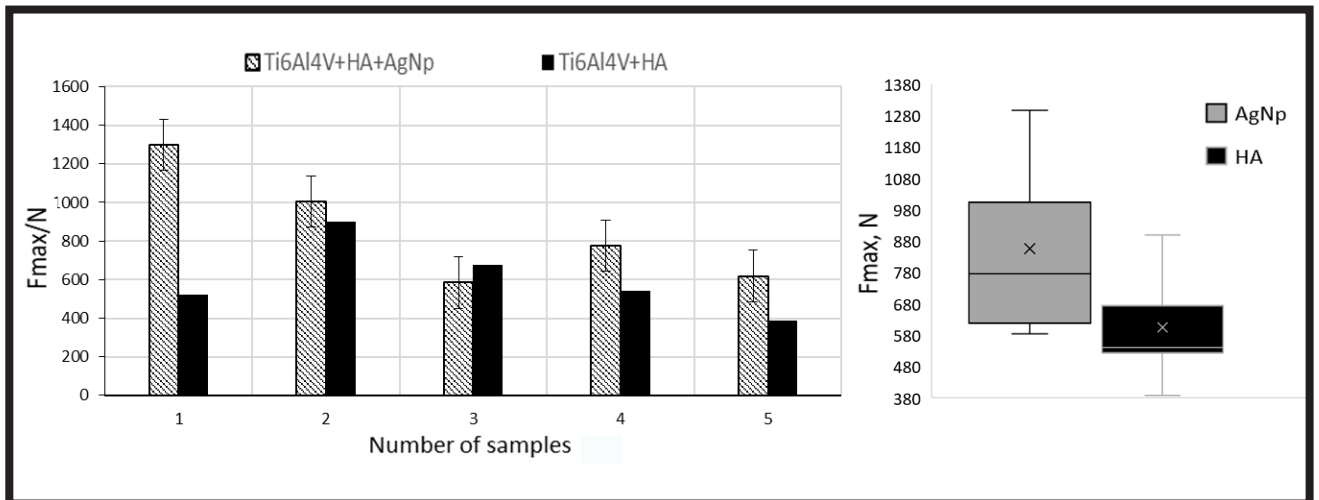
FIG. 9. Values of forces needed to pull out implants with standard deviation (A) and results of statistical analysis (B).

The implants did not induce any negative or unexpected reactions within the adjacent soft tissues or bones. After two months, the implants were removed – FIG. 9 shows the values of the forces needed to remove the implants from the bone.

When interpreting the obtained data, it was found that the extraction force for the implants was different and for both groups of implants it ranged from 388 to 1297 N. The extraction force for the implants with the hydroxyapatite coating and silver nanoparticles was slightly higher when compared to the implants with the hydroxyapatite coating. The mean, without the extreme values, was 800 N and 580 N, respectively for the Ti6Al4V+HA+AgNp and Ti6Al4V+HA implants. The median value for the AgNp samples was 775 N, and for HA was 541 N. The box graph (FIG. 9B) shows the dispersion of the results obtained and indicates that the data obtained was asymmetrical. Despite the large dispersion of results for the AgNp samples, the smallest value for the AgNp sample (585 N) was still greater than the median for HA samples.

The formation of the strong implant-bone bonding is critical to the clinical success of orthopedic procedures. The structure of the implant surface can play a decisive role in creating such a bonding. A rough surface and open pores of the coating favour the formation of a strong adhesive bond between the implant and the bone due to tissue interference in the implant interior and its connection to the bone. In [16] the authors state that strong bone overgrowth is also associated with the method of coating application and the lower residual stress occurring in the HA coating.

In the presented study, the implants surface modification positively influenced the obtained stabilization value, in comparison with the implants with the reference surface, i.e. covered only with hydroxyapatite. Although the antimicrobial properties of AgNp are well documented, their effect on the osseointegration of orthopedic implants is not well understood [17]. Nevertheless, it is believed that the presence of silver nanoparticles accelerates the healing process and reduces the duration of inflammation. Due to this phenomenon, bone cells start to overgrow faster, creating a stronger connection. The findings suggest a beneficial effect of silver nanoparticles on processes occurring in the peri-implant area, but this requires confirmation in further studies. The authors are aware that the tests should be carried out on a larger number of samples, but for ethical reasons, they have been carried out on the smallest possible number of animals.

Conclusions

The following conclusions were made on the basis of the conducted research:
- as a result of applying HA, a coating was obtained that complies with the specification of the plasma spray process,
- on the hydroxyapatite coating with silver nanoparticles, a homogeneous distribution of silver nanoparticles with sporadically occurring agglomerates is observed,
- with the extension of the sample incubation time, an increasing number of ions is released into the liquid and this process occurs gradually,
- surface modification with silver nanoparticles has a positive effect on the implant stability in the bone. The average force (without the extreme values) needed to remove the implant with the HA+AgNp coating from the bone is 800 N, which is 220 N higher when compared to the implants with the reference surface.

Acknowledgments

ORCID iDs

J. Sulej-Chojnacka: https://orcid.org/0000-0003-0158-7125
W. Woźniak: https://orcid.org/0000-0002-8173-131X
D. Andrzejewski: https://orcid.org/0000-0003-0798-1676

References

[1] Gierzyńska-Dolna M., Lijewski M.: Badania tribologicznych właściwości biomateriałów i implantów. Obróbka Plastyczna Metali XXIII Nr 3 (2012).

[2] Borkowski L., Pawłowska M., Polkowska I., Karpiński M., Słowik T., Piersisk T., Matuszewski Ł., Ślósarczyk A., Ginalska G.: Histological and radiological analysis of rabbit bones after implantation of CHAP-glucan composite. Engineering of Biomaterials 114 (2012) 28-33.

[3] Karlsson J., Jimbo R., Fathali H.M, Schwartz-Filho H.O., Hayashi M., Halvarsson M., Wennerberg A., Andersson M.: In vivo biomechanical stability of osseointegrating mesoporous TiO$_2$ implants. Acta Biomaterialia 8 (2012) 4438-4446.

[4] Dan-Jae L., Chien-Ping J., Shu-Huei H., Yin-Chun T., Hsiang-Shu Y., Wen-Cheng Ch., Jiin-Huey Ch.L.: Mechanical testing and osteointegration of titanium implant with calcium phosphate bone cement and autograft alternatives. Journal of the mechanical behavior of biomedical materials 4 (2011) 1186-1195.

[5] Makuch K., Koczorowski R.: Biokompatybilność tytanu oraz jego stopów wykorzystywanych w stomatologii. Dent. Med. Probl. 47(1) (2010) 81-88.

[6] Chung C.J., Su R.T., Chu H.J., Chen H.T., Tsou H.K., He J.L.: Plasma electrolytic oxidation of titanium and improvement in osseointegration. Journal of Biomedical Materials Research Part B: Applied Biomaterials 101(6) (2013) 1023-1030.

[7] Zhang X., Chaimayo W., Yang C., Yao J., Miller B.L., Yates M.Z.: Silver-hydroxyapatite composite coatings with enhanced antimicrobial activities through heat treatment, Surface & Coatings Technology 325 (2017) 39-45.

[8] Agarwal R., García A.J.: Biomaterial strategies for engineering implants for enhanced osseointegration and bone repair: Advanced Drug Delivery Reviews 94 (2015) 53-62.

[9] Speruda M., Kędziora A., Bugla-Płoskońska G.: Antybakteryjne działanie nanocząstek srebra syntetyzowanych metodą zielonej chemii. Medycyna Doświadczalna i Mikrobiologia 69 (2017) 281-288.

[10] Song L., Xiao Y.F., Gan L., Wu Y., Wu F., Gu Z.W.: The effect of antibacterial ingredients and coating microstructure on the antibacterial properties of plasma sprayed hydroxyapatite coatings. Surface and Coatings Technology 206(11-12) (2012) 2986-2990.

[11] Guzman M., Dille J., Godet S.: Synthesis and antibacterial activity of silver nanoparticles against gram-positive and gram-negative bacteria. Nanomedicine: Nanotechnology, Biology, and Medicine 8 (2012) 37-45.

[12] Salem W.M., Haridy M., Sayed W.F., Hassan N.H.: Antibacterial activity of silver nanoparticles synthesized from latex and leaf extract of Ficus sycomorus. Industrial Crops and Products 62 (2014) 228-234.

[13] Ziąbka M., Merta A., Król W., Bobrowski A., Chłopek J.: High Density Polyethylene Containing Antibacterial Silver Nanoparticles for medical Applications. Macromolecular Symposia 315 (2012) 218-225.

[14] Dubnika A., Loca D., Rudovica V., Bharat Parekh M., Berzina-Cimdina L.: Functionalized silver doped hydroxyapatite scaffolds for controlled simultaneous silver ion and drug delivery. Ceramics International 43(4) (2017) 3698-3705.

[15] Li J., Jansen J.A., Walboomers X.F., van den Beucken J.J.: Mechanical aspects of dental implants and osseointegration: A narrative review. Journal of the mechanical behavior of biomedical materials 103 (2020) 103574.

[16] Yang Y.Ch., Yang Ch.Y.: Mechanical and histological evaluation of a plasma sprayed hydroxyapatite coating on a titanium bond coat. Ceramics International 39 (2013) 6509-6516.

POLYMERIZATION SHRINKAGE OF RESIN MIXTURES USED IN DENTAL COMPOSITES

Krzysztof Pałka[1*] (iD), Patrycja Janiczuk[1] (iD),
Joanna Kleczewska[2] (iD)

[1] Lublin University of Technology,
Faculty of Mechanical Engineering,
Nadbystrzycka 36, 20-618 Lublin, Poland
[2] Arkona Laboratory of Dental Pharmacology,
Nasutów 99C, 21-025 Niemce, Poland
*e-mail: k.palka@pollub.pl

Abstract

Polymerization of dental composites generates shrinkage in the matrix resulting in numerous clinical problems. The influence of the most commonly used resins on the shrinkage process has not been thoroughly examined so far in the literature. The purpose of this work is to determine the effect of the resin mixture compositions on the volumetric polymerization shrinkage. The mixtures used in the tests were prepared in specific weight proportions to determine the influence of particular monomers, such as Bis-GMA, Bis-EMA, UDMA, and TEGDMA. The shrinkage measurements were performed using the self-designed video-imaging device. The studies showed that the shrinkage decreased in opposite to the Bis-GMA concentration in the mixture with the simultaneous decrease in the Bis-EMA content. The shrinkage value decreased in opposite to the molecular weight only for some monomers and compositions. Bis-EMA resin as a flexible monomer achieved the lower shrinkage values than UDMA, and the highest shrinkage values, above 6%, were achieved by compositions with the 14wt% content of Bis-GMA. Regarding the shrinkage, the most optimal composition was 56wt% Bis-GMA with the addition of Bis-EMA (24wt%) and TEGDMA (20wt%). The obtained shrinkage value was 4.73%.

Keywords: *polymer blends, volumetric shrinkage, dimetacrylates, dental composite*

Introduction

Light-curable dental composites are currently the most commonly used materials for the direct reconstruction of enamel and dentin, accounting for about 70% of all dental restorations [1]. They are made of a polymer matrix reinforced with organic or inorganic, mineral, or mixed particles [2]. From the 1960's, with the invention of the Bis-GMA monomer by Bowen, they became the main direction of development in aesthetic dentistry, gradually replacing amalgams, cements and restorations made of precious metals [3]. The universality in the use of composites based on light-curable resins is primarily implied by their beneficial mechanical properties, wear resistance, durability, ease of application and aesthetic [1].

In addition to regaining the functionality of the teeth and guaranteeing their aesthetic appearance, composite restorations perform a very important function which is reducing the risk of health-threatening infections associated with the development of caries [4]. The key factor in maintaining the marginal adaptation and durability of these restorations turns out to be the polymerization shrinkage, resulting from the exchange of van der Waals intermolecular interactions to covalent bonds between monomers during polymerization. As a consequence of this phenomenon, stresses arise in the restoration-tooth interface, worsening adhesion and leading to the formation of a marginal fissure where bacteria can enter causing secondary caries [2]. Stresses exceeding the enamel strength may lead to a fracture within the bond with the material [5,6].

Most composites used in restorative dentistry shrink linearly by 0.6-1.4% [7], however, the value of volumetric contraction may be as high as 7% [8]. The polymerization shrinkage depends on the resin composition as well as the amount of filler particles and radiation intensity [9]. The size of the polymerization shrinkage depends, among others, on the molecular weight and functionality of the monomers. When comparing monomers with the same molecular weight, the polymerization shrinkage increases with functionality. Comparing monomers with the same functionality, the polymerization shrinkage increases opposite to the molecular weight, as a consequence, mixtures of Bis-GMA and other monomers will affect the polymerization shrinkage [10]. The purpose of this work is to determine the effect of resin mixture composition on the volumetric polymerization shrinkage.

Materials and Methods

In order to assess the relationship between the composition of the resins mixtures used as the matrix of dental composites and the resulting polymerization shrinkage, compositions with a suitably wide range of resin proportions were prepared, and then subjected to shrinkage tests at the designed stand and via the authors' own method.

The four most popular dimethacrylate resins: Bis-GMA (CAS 1565-94-2), Bis-EMA (CAS 41637-38-1), UDMA (CAS 72869-86-4) and TEGDMA (CAS 109-16-0) were mixed in the proportions shown in TABLE 1. The weight ratios for the mixtures and their markings are shown in TABLE 2.

TABLE 1. Physical properties of tested dimethacrylates.

| Monomer	Molecular weight (average)	Double bond concentration (mol/kg)	Viscosity (Pa·s)
Bis-GMA	510.6	3.90	1200.00
Bis-EMA	540.0	3.70	0.90
UDMA	470.0	4.25	23.10
TEGDMA	286.3	6.99	0.01

Each mixture contained camphorquinone (an initiator; CAS 10373-78-1) and N,N-dimethylaminoethyl methacrylate (CAS 2867-47-2) as a *co*-initiator for light-cured free-radical polymerization, as well as 20wt% of the TEGDMA, which acts as an active solvent decreasing the viscosity of the mixture and facilitating effective mixing. The amount of TEGDMA monomer was constant for all the tested mixtures. The compositions were prepared by mixing precisely weighed ingredients (± 0.1 mg) using the WAS 220 laboratory balance (Radwag). The mixing process was carried out under low energy lighting to avoid an accidental polymerization of the resins.

The shrinkage measurements were carried out on the self-designed video-imaging device which is schematically presented in FIG. 1. The specimen was deposited on the stainless steel pin of the 3 mm diameter. The top surface of the pin was placed in the optical axis of the camera to minimize the geometrical deformations of the acquired image. The pin with the resin droplet was rotated during the measurement in a full angle range with the step of 20°, realized by a stepper motor controlled by the dedicated software. In each angular position, an image (640x480 pixels) was taken until the last position of the sample was reached. The image acquisition was also controlled by the software. Yellow diffused light was used to obtain good exposure conditions (without reflections) and to avoid accidental curing.

TABLE 2. Resin compositions used to measure polymerization shrinkage. Each specimen contained 20wt% of TEGDMA.

Specimen	Bis-GMA (wt%) (G)	Bis-EMA (wt%) (E)	UDMA (wt%) (U)
G	80.0	-	-
E	-	80.0	-
U	-	-	80.0
G40E40	40.0	40.0	-
G56E24	56.0	24.0	-
G24E56	24.0	56.0	-
G40U40	40.0	-	40.0
G56U24	56.0	-	24.0
G24U56	24.0	-	56.0
G27E27U27	26.7	26.7	26.7
G26E40U14	26.0	40.0	14.0
G26E14U40	26.0	14.0	40.0
G14E26U40	14.0	26.0	40.0
G40E26U14	40.0	26.0	14.0
G40E14U26	40.0	14.0	26.0
G14E40U26	14.0	40.0	26.0
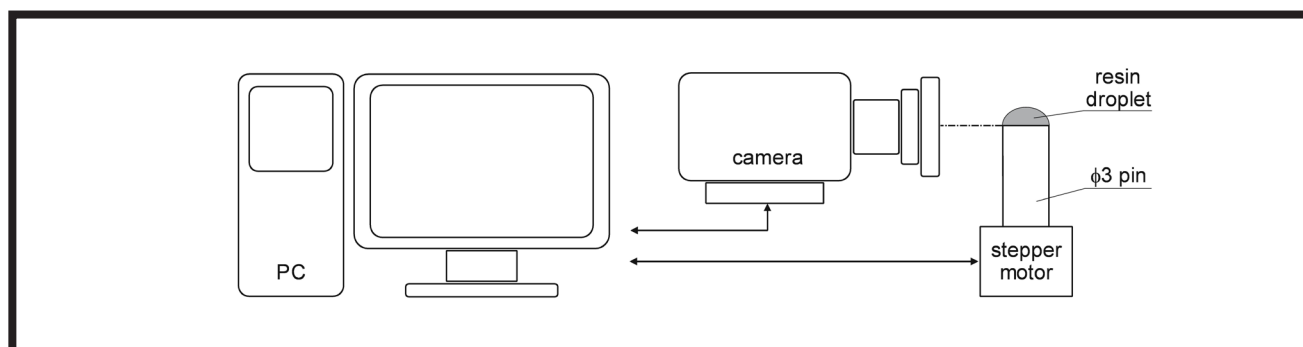
FIG. 1. The idea of the measuring system.

The resin polymerization was performed right after the first scan (of the uncured resin) followed by the second scan of the specimen. The halogen lamp Cromalux 75 (Mega-Physik) was used for curing for 20 sec. A set of 18 images of each scan was then analyzed in order to obtain the sample volume.

The sample volume was measured from the projection of the samples' visible area. The volume of such a rotational figure can be determined as the product of the half surface area *A* (indicated by the axis of rotation) and the radius of its rotation *r*. The radius of rotation *r* was established as the distance of the analyzed figure centroid from the axis of rotation (FIG. 2a). The area *A* was measured by image analysis. All the measurements were carried out in the CTAnalyser software (Bruker microCT). The measurements were taken with an accuracy of 6.6 μm for 10 samples of each resin type (each measurement for 18 + 18 images in total) and the results were statistically analyzed using the Statistica software (TIBCO Software Inc.) at the confidence level α<0.05. Superimposing images taken before and after curing revealed the material loss due to shrinkage (FIG. 2b).
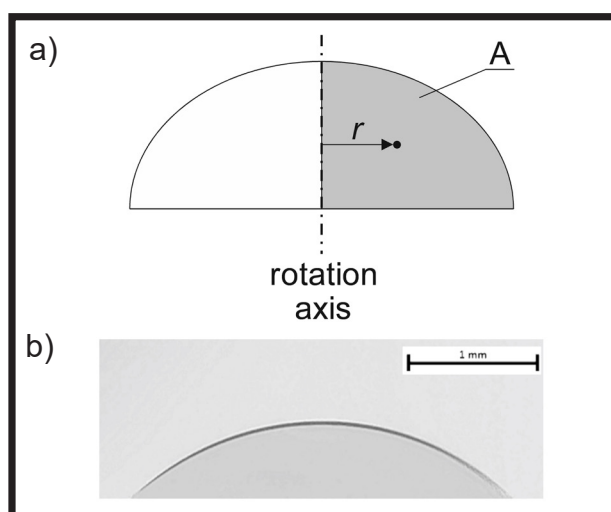
FIG. 2. a) The principle of determining data for volume calculations, b) trace of material loss after superimposing images before and after curing.

The volumetric polymerization shrinkage was calculated as follows:

$$S_V = \frac{V_1 - V_2}{V_1} \cdot 100\% \qquad (1)$$

where: V_1 is the initial droplet volume and V_2 is the droplet volume of the material after polymerization.

Such a method is suitable especially for materials of relatively low viscosity, which allows them to spread freely over the pin surface and create a symmetrical drop.

Results and Discussions

The results of volumetric shrinkage for the mixtures based on Bis-GMA, Bis-EMA, UDMA, and TEGDMA are presented in FIG. 3 and TABLE 3 which also presents the standard deviation values and the variation coefficient. The material G presented the lowest shrinkage and at the same time the highest deviation. However, among all the tested samples, deviation remained low.

The varied properties of the used materials, such as viscosity, double bond concentration, and in particular the molecular weight of the monomer (TABLE 1) determine the shrinkage value generated in the polymer. Unlike UDMA and TEGDMA, the Bis-GMA as well as Bis-EMA resins have approximately the same molecular weight, and therefore a higher concentration of double bonds. According to the work [4], the main factors that affect shrinkage are: the conversion degree, the molecular weight of the monomer and the type and amount of the used reinforcement (for composites). The polymerization shrinkage increases with the conversion degree and decreases with the increasing monomer molecular weight and the decreasing double bond concentration.

According to the above statement, the G composition achieved the lowest contraction among the subjects. It contained 80% by weight Bis-GMA which has a high mass and a relatively low number of double bonds. The shrinkage value increased successively for the E and U compositions together with the decrease in the double bond concentration. Sideridou et al. [11] examined the conversion degree for dimethacrylates, such as Bis-GMA, Bis-EMA, UDMA and TEGDMA, and obtained an upward trend for the resins, respectively.

TABLE 3. Results of volumetric shrinkage measurements.

Mixture	Volumetric shrinkage [%]	S.D. [%]	Coefficient of variation [%%]
G	3.51	0.63	17.93
E	4.73	0.66	13.95
U	5.55	0.62	11.17
G40E40	5.00	0.48	9.60
G56E24	4.73	0.56	11.88
G24E56	5.65	0.63	11.15
G40U40	5.49	0.66	12.02
G56U24	5.37	0.33	6.20
G24U56	5.01	0.53	10.58
G27E27U27	5.51	0.34	6.23
G26E40U14	5.45	0.61	11.20
G26E14U40	4.84	0.44	9.09
G14E26U40	6.10	0.58	9.45
G40E26U14	5.42	0.47	8.61
G40E14U26	5.44	0.42	7.71
G14E40U26	6.22	0.54	8.74

The trend was explained by the claim that the conversion degree increases with the increasing polymerization shrinkage, as evidenced by the test results for the analogous G, E, and U materials. In the work of Yoon [12], the studies of Bis-GMA monomer shrinkage were found by the density determination. The obtained result of 3.4 ± 0.3%, was approximate to the result of our work. The above results confirmed the reliability of the measuring method presented in this paper.

Only four of the sixteen compositions achieved the shrinkage level below 5%: G, E, G56E24, and G26E14U40. The mixtures containing Bis-GMA and Bis-EMA were the majority in these materials. However, the result obtained for the G26E14U40 sample, which contained only 40wt% of Bis-GMA and Bis-EMA, was unexpected. The standard deviation for this sample was 0.44% and its shrinkage value was similar to the other materials.
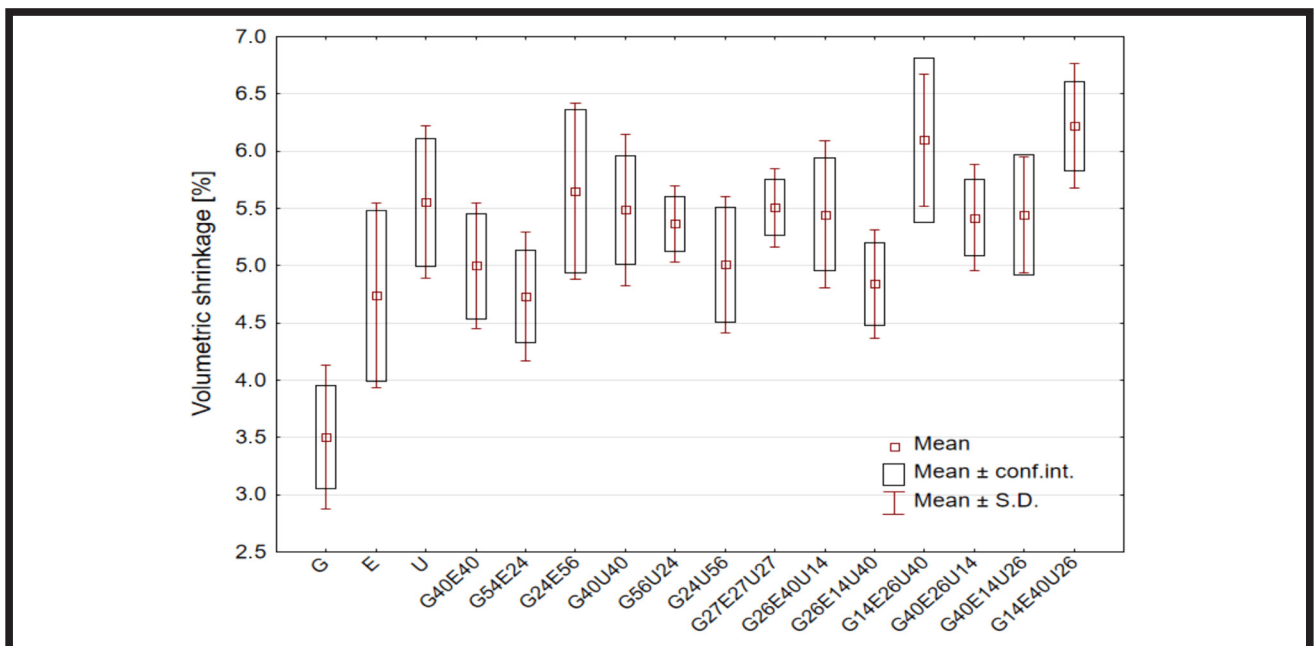

FIG. 3. Results of volumetric shrinkage measurements.

TABLE 4. Probability values *p* from the *t* test. Statistically significant differences at *p*<0.05.

	E	U	G40E40	G56E24	G24E56	G40U40	G56U24	G24U56	G27E27U27	G26E40U14	G26E14U40	G14E26U40	G40E26U14	G40E14U26	G14E40U26
G	0.003	0.000	0.000	0.000	0.000	0.000	0.000	0.000	0.000	0.000	0.000	0.000	0.000	0.000	0.000
E	1.000	0.051	0.471	0.981	0.051	0.052	0.041	0.467	0.016	0.070	0.755	0.009	0.043	0.090	0.000
U		1.000	0.091	0.012	0.795	0.841	0.448	0.107	0.854	0.744	0.021	0.160	0.621	0.744	0.032
G40E40			1.000	0.324	0.079	0.112	0.098	0.971	0.028	0.146	0.530	0.005	0.098	0.146	0.000
G56E24				1.000	0.012	0.013	0.006	0.323	0.002	0.019	0.651	0.001	0.008	0.023	0.000
G24E56					1.000	0.648	0.311	0.092	0.608	0.573	0.021	0.301	0.448	0.586	0.093
G40U40						1.000	0.607	0.130	0.937	0.891	0.026	0.104	0.786	0.889	0.014
G56U24							1.000	0.126	0.362	0.731	0.011	0.008	0.777	0.713	0.000
G24U56								1.000	0.040	0.168	0.523	0.008	0.121	0.175	0.000
G27E27U27									1.000	0.799	0.002	0.026	0.632	0.767	0.003
G26E40U14										1.000	0.036	0.086	0.912	0.993	0.011
G26E14U40											1.000	0.001	0.015	0.033	0.000
G14E26U40												1.000	0.028	0.075	0.691
G40E26U14													1.000	0.918	0.002
G40E14U26														1.000	0.013

The 5% shrinkage was demonstrated for the *G40E40* and *G24U56* samples. The shrinkage above 6% was achieved by two compositions: *G14E26U40* and *G14E40U26* containing the smallest amount of Bis-GMA among all the tested materials. These materials displayed the highest volumetric shrinkage. The difference in the average shrinkage value of the *G14E40U26* sample was not statistically significant only when compared to the average of the *G14E26U40* sample. The results of the *t* test, carried out in Statistica, for all the compositions are presented in TABLE 4.

Effect of varied two resins proportions on shrinkage

The test results confirmed the literature reports that the higher molecular weight of the monomer generated lower polymerization shrinkage. The obtained results were consistent with the literature data [7,9] regarding resins with the variable concentration of Bis-GMA and TEGDMA. In the *U* composition, 80% by weight of the Bis-GMA monomer was replaced by the same amount of UDMA monomer that had over 40% lower weight, thus obtaining the 2% higher shrinkage.

The above statement is contradictory to the analysis of the Bis-EMA shrinkage results because the resin has a higher molecular weight than Bis-GMA and the obtained shrinkage is higher. The difference between the result obtained for the *G* sample with the highest concentration of Bis-GMA and Bis-EMA as well as the other results is statistically significant, as demonstrated by the *t* test. The analysis of the above results is shown in FIG. 4. In addition, a significant shrinkage increase was noted with a gradual increase in the Bis-EMA monomer content and the decrease in Bis-GMA concentration. The proportions visible in the chart do not include the weight content of the TEGDMA resin. The mass concentrations are assumed relatively to the materials considered in a given context.

As for the relationship between compositions, it must be noted that the difference between the mean values of volumetric shrinkage for *G40E40* and *G56E24* was not statistically significant. The difference in the shrinkage value between the mixtures containing 30wt% Bis-EMA and the 70wt% Bis-Ema was approximately 1%. Despite the higher molecular weight (540 g/mol), the ethoxylated version of Bis-GMA did not have such strong molecular interactions occurring due to the existence of hydroxyl groups, which reduced its viscosity and resulted in the higher conversion degree and thus the higher polymerization shrinkage [13]. Therefore, the thesis cited in many papers about the dependence of the shrinkage on the molecular weight of the monomer was not confirmed for all types of resins.

In turn, the results obtained by Sideridou et al. showed the lower conversion degree for materials with a higher concentration of Bis-GMA monomer which is associated with a small number of double bonds and high system viscosity. The hydroxyl groups contained in Bis-GMA molecules are capable of forming intermolecular hydrogen bonds, which in turn limit the slip of polymer chains. Fewer double bonds are transformed, gradually increasing the system viscosity as the Bis-GMA content in the composite increases. Limiting the increasing mobility of macro-radicals and monomers affects the propagation of free radicals and thus reduces the conversion degree [11].

Varied concentrations of Bis-GMA and UDMA were used in the *G40U40*, *G56U24*, and *G24U56* compositions. The shrinkage results were inconclusive for these two monomers endowed with different properties. Although both monomers are relatively large molecular structures, Bis-GMA prevails in terms of molecular weight and also has significant conversion restrictions [14] which the polymerization progress is related to. Therefore, a partial replacement of the Bis-GMA monomer in the composite may be essential to optimizing the resin composition.
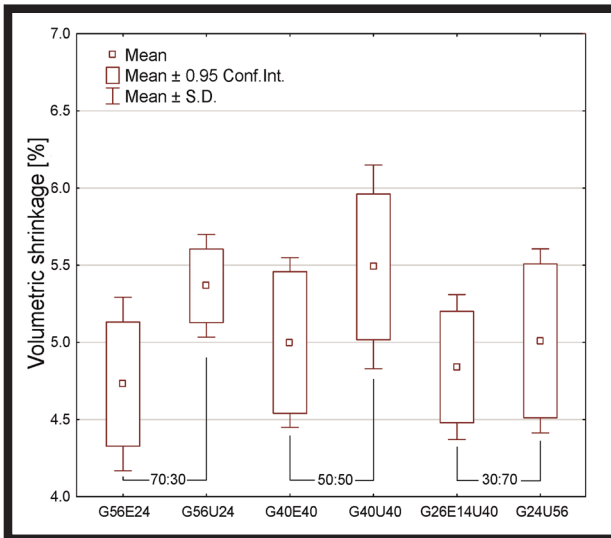
FIG. 4. Polymerization shrinkage of resins containing a constant amount of 20% TEGDMA with variable Bis-GMA:Bis-EMA and Bis-GMA:UDMA rates.
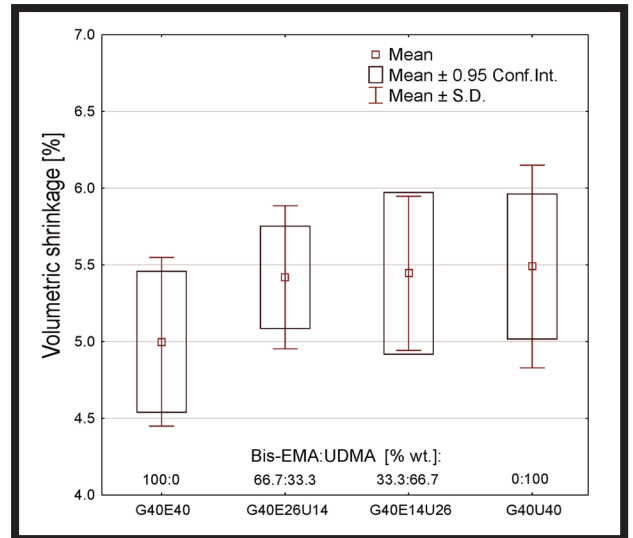

FIG. 5. Volumetric shrinkage of resins with a constant concentration of Bis-GMA (40wt%) containing a variable fraction of Bis-EMA:UDMA.
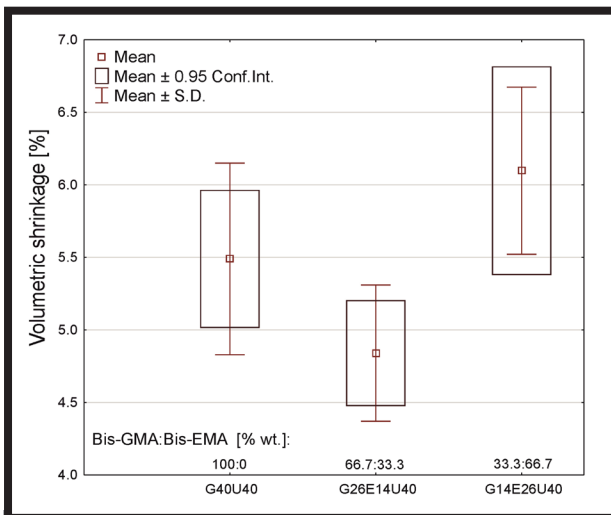
Effect of the proportion variability of three resins on shrinkage

Polymerization leads to only a partial reaction of the double bonds, which is perceived as a negative phenomenon [17]. Under such conditions, only very flexible monomers undergo the complete conversion. Among the resins with the relatively low viscosity used in commercial composites are Bis-EMA and UDMA as an alternative to TEGDMA. Identification of new flexible monomers is necessary since TEGDMA contributes to the increasing polymerization shrinkage in composites [7]. The Bis-EMA monomer has a slightly higher molecular weight and the lower concentration of double bonds in the structure than the UDMA monomer, which is also reflected in the achieved value of shrinkage (FIG. 5).

The test results showed a correlation between the shrinkage and concentration of Bis-EMA and UDMA. The volumetric shrinkage slightly increased with the concentration of UDMA. There was a statistically significant difference between the average values for the *G40E40* and the *G40E14U26* samples. There were no statistically significant differences between the other tested samples. The *G40E40* sample, without UDMA, obtained a relatively low shrinkage of 5%. To summarize, Bis-EMA as a monomer of moderate viscosity was more effective than UDMA in reducing the shrinkage.

The effect on the shrinkage performed by the Bis-GMA and Bis-EMA concentrations with the constant UDMA and TEGDMA content is explained in FIG. 6. The molecular weight of the presented compositions increased together with the Bis-EMA content. It resulted in the shrinkage increase similarly to the compositions with two resins. However, the lack of Bis-EMA in the *G40U40* composition led to the even greater shrinkage than its 14wt% addition. Again, the molecular weight was not the reason for the value of generated shrinkage.

The highest 6% shrinkage was obtained for the *G14E26U40* and *G14E40U26* materials containing the smallest amount of Bis-GMA, which was replaced by Bis-EMA, UDMA and TEGDMA monomers. The most optimal composition, containing a relatively small amount of Bis-GMA, and achieving the shrinkage of less than 5% was the *G26E14U40* mixture. The same Bis-GMA content but a different UDMA and Bis-EMA monomers proportion of did not guarantee a result below 5% (*G26E40U14*).

FIG. 6. Polymerization shrinkage of resins containing a constant 40% UDMA and 20% TEGDMA, with a variable rate of Bis-GMA:Bis-EMA.

A low conversion leads to the transfer of unreacted components to soft tissue and causes irritation [11,15] and such restorations have a lower clinical performance [16]. Due to the high viscosity of Bis-GMA, the addition of another more flexible monomer is recommended. For the 50/50 concentration, the highest shrinkage of 5.37% was obtained of the three samples, but no statistical significance was observed for all the results. Despite this, Ferracane [7] revealed the decreasing shrinkage with the increasing UDMA concentration in the mixture, which occurred in the results of the *G56U24* and *G24U56* samples. However, replacing Bis-GMA with 70% UDMA still did not lead to the low shrinkage values represented by sample *G* (80% by weight Bis-GMa, 20% by weight TEGDMA) but reduced it by almost 0.4% as compared to the 30wt% content.

Considering the series of samples with the same proportion variation (FIG. 4) where Bis-GMA is replaced by Bis-EMA or UDMA, two of the three samples achieved the lower shrinkage values for the Bis-EMA substitute. Moreover, in the case of the *G56E24* composition with the 70:30 Bis-GMA and Bis-EMA ratio the obtained shrinkage value was the second smallest.

Conclusions

The polymerization shrinkage is one of the most important properties of dental composites, but its level is still unsatisfactory in the context of generated stresses and clinical durability of restorations. The measurements of the polymerization shrinkage of the Bis-GMA, UDMA, Bis-EMA and TEGDMA resins in varying weight proportions allowed us to determine the following relationships:

The decreasing shrinkage as the molecular weight of the monomer increases was not the rule. Apart from the molecular weight of resin, other properties such as the resin viscosity, the double bond concentration and the presence of the filler, also could have an influence on the composite shrinkage.

The shrinkage decreased with the increasing Bis-GMA and simultaneous decreasing of Bis-EMA concentration in the mixture.

The compositions containing 14wt% of Bis-GMA achieved the highest shrinkage values, above the 6wt%. However, the increase in the Bis-GMA concentration to 24% and the addition of a specific amount of Bis-EMA and TEGDMA reduced the shrinkage below 5% and such compositions seem to be the optimal ones.

Considering the polymerization shrinkage, Bis-EMA is a better alternative to TEGDMA than UDMA.

Acknowledgements

ORCID iDs

K. Pałka: https://orcid.org/0000-0003-4920-4613
P. Janiczuk: https://orcid.org/0000-0002-7806-2944
J. Kleczewska: https://orcid.org/0000-0002-9149-3597

References

[1] Braga R.R., Ballester R.Y., Ferracane J.L.: Factors involved in the development of polymerization shrinkage stress in resin-composites: A systematic review. Dental Materials 21 (2005) 962-970. https://doi.org/10.1016/j.dental.2005.04.018
[2] Rüttermann S., Dluzhevskaya I., Großsteinbeck C., Raab W.H.M., Janda R.: Impact of replacing Bis-GMA and TEGDMA by other commercially available monomers on the properties of resin-based composites. Dental Materials 26 (2010) 353-359. https://doi.org/10.1016/j.dental.2009.12.006
[3] Schneider L.F.J., Cavalcante L.M., Silikas N.: Shrinkage stresses generated during resin-composite applications: A review. Journal of Dental Biomechanics 1 (2010) 1-14. https://doi.org/10.4061/2010/131630
[4] Lemon M.T., Jones M.S., Stansbury J.W.: Hydrogen bonding interactions in methacrylate monomers and polymers. Journal of Biomedical Materials Research - Part A 83 (2007) 734-746. https://doi.org/10.1002/jbm.a.31448
[5] Pałka K., Bieniaś J., Dębski H., Niewczas A.: Finite element analysis of thermo-mechanical loaded teeth. Computational Materials Science 64 (2012) 289-294. https://doi.org/10.1016/j.commatsci.2012.05.037
[6] Dębski H., Bieniaś J., Pałka K., Niewczas A.: Analysis of stress level in hard dental tissues using finite element method. Engineering of Biomaterials/Inżynieria Biomateriałów 112 (2012) 42-47.
[7] Ferracane J.L.: Resin composite - State of the art. Dental Materials 27 (2011) 29-38. https://doi.org/10.1016/j.dental.2010.10.020
[8] Chuang S., Huang P., Chen T.Y.: Shrinkage behaviors of dental composite restorations - The experimental – numerical hybrid. Dental Materials, The Academy of Dental Materials. 32 (2016) e362-373. https://doi.org/10.1016/j.dental.2016.09.022
[9] Yin M., Liu F., He J.: Preparation and characterization of Bis-GMA free dental resin system with synthesized dimethacrylate monomer TDDMMA derived from tricyclo[5.2.1.0(2,6)]-decanedimethanol. Journal of the Mechanical Behavior of Biomedical Materials 57 (2016) 157-163. https://doi.org/10.1016/j.jmbbm.2015.11.020

[10] Peutzfeldt A.: Resin composites in dentistry: The monomer systems. European Journal of Oral Sciences 105 (1997) 97-116. https://doi.org/10.1111/j.1600-0722.1997.tb00188.x
[11] Sideridou I., Tserki V., Papanastasiou G.: Study of water sorption, solubility and modulus of elasticity of light-cured dimethacrylate-based dental resins. Biomaterials 24 (2003) 655-665. https://doi.org/10.1016/S0142-9612(02)00380-0
[12] Yoon T.H., Lee Y.K., Lim B.S., Kim C.W.: Degree of polymerization of resin composites by different light sources. Journal of Oral Rehabilitation 29 (2002) 1165-1173. https://doi.org/10.1046/j.1365-2842.2002.00970.x
[13] Lewandowska M., Andrzejczuk M., Kurzydłowski K.J., Karaś J., Szafran M., Rokicki G.: Kompozyty ceramiczno-polimerowe stosowane na stałe wypełnienia stomatologiczne - wpływ cząstek wypełniacza na właściwości mechaniczne. Kompozyty 4 (2004) 302-305.
[14] Marciniak J., Kaczmarek M., Ziębowicz A.: Biomateriały w stomatologii. Wydawnictwo Politechniki Śląskiej, Gliwice (2008).
[15] Palin W.M., Fleming G.J.P., Burke F.J.T., Marquis P.M., Randall R.C.: The influence of short and medium-term water immersion on the hydrolytic stability of novel low-shrink dental composites. Dental Materials 21 (2005) 852-863. https://doi.org/10.1016/j.dental.2005.01.004
[16] Ito S., Hashimoto M., Wadgaonkar B., Svizero N., Carvalho R.M., Yiu C. et al.: Effects of resin hydrophilicity on water sorption and changes in modulus of elasticity. Biomaterials 26 (2005) 6449-6459. https://doi.org/10.1016/j.biomaterials.2005.04.052
[17] Sun J., Lin-Gibson S.: X-ray microcomputed tomography for measuring polymerization shrinkage of polymeric dental composites. Dental Materials 24 (2008) 228-234. https://doi.org/10.1016/j.dental.2007.05.001

PREPARATION AND CHARACTERISTICS OF POLYURETHANE-BASED COMPOSITES REINFORCED WITH BIOACTIVE CERAMICS

Natalia Złocista-Szewczyk, Piotr Szatkowski (iD),
Kinga Pielichowska* (iD)

AGH University of Science and Technology,
Faculty of Materials Science and Ceramics,
Department of Biomaterials and Composites,
al. A. Mickiewicza 30, 30-059 Kraków, Poland
*e-mail: kingapie@agh.edu.pl

Abstract

The purpose of the study was to synthesize and characterize a series of porous polyurethane-based composites modified with β-tricalcium phosphate (TCP) and hydroxyapatite (HAp). The composites were obtained by the one-step bulk polyaddition method using poly(ethylene glycol) (PEG) as a soft segment, 4,4'-diphenylmethane diisocyanate (MDI), 1,4-butanediol (BDO) as a chain extender and selected bioactive bioceramics. The obtained composites were characterized using FTIR, DSC, TG and SEM/EDX methods. Moreover, in vitro chemical stability and wettability tests were performed. The preliminary assessment of mechanical properties, porosity and in vitro chemical stability was performed. The test results showed that the best pore distributions, as well as Young's modulus, were found for the hydroxyapatite-modified composites and PU/20% TCP. The wettability investigations revealed that the contact angle of PU composites was in the range 50-80°, which indicates the hydrophobic nature of the materials. The in vitro biostability studies confirmed that all tested composites were chemically stable during incubation in the simulated body fluid. By using infrared spectroscopy the presence of urethane bonds and completion of reaction were evidenced. The results showed that the bioactivity of the materials was improved, which makes good perspectives for the obtained materials to be considered as potential scaffolds in bone tissue regeneration.

Keywords: *polyurethane, HAp, TCP, orthopaedics, bone regeneration*

Introduction

One of the observed trends in the development of medicine is the biomimetic approach. Currently, studies are performed on materials imitating human tissues, such as bone. Different types of materials and implants not only perform mechanical functions but also facilitate the regeneration of damaged tissues.

The bone tissue can be considered as a nanocomposite of an organic collagen matrix, reinforced with an inorganic phase - hydroxyapatite (HAp). Having been damaged, the bone tissue exhibits a very high self-healing ability. However, there is a critical size of the loss which the bone is not able to heal properly [1-3]. Resorbable polymers are most commonly used as they can stabilize the damaged tissue and then degrade in the body. During the gradual resorption, they simultaneously release the medicaments, such as antibiotics or proteins [1,4]. One of the most promising polymers for bone tissue regeneration are polyurethanes (PU). Polyurethane-based materials for bone tissue regeneration and replacement have been widely studied in recent years. Hence, in the work by Gabard et al. [5], PU modified with HAp nanocrystals was described. They showed that the addition of nanoHAp reduced the surface energy of the material, which made it possible to control the initial absorption of the protein and simultaneously inhibit the spread of inflammatory cells. The tests confirmed the material's high decomposition temperature, which enables the proper sterilization. Biological studies revealed biocompatibility in both in vitro and in vivo conditions. The foam composite made of PU modified with bioglass was investigated by Ryszkowska et al. [6]. The porosity of the obtained composite meets the requirements for bone tissue engineering. Additionally, the material has a high biological activity, which was confirmed by incubation in the simulated body fluid (SBF) when apatites were formed on the foam surface. Dulińska-Molak et al. [7] studied PU filled with calcite composites. They found that ceramic composites based on polyurethanes exhibited better properties as implants than the unfilled materials. The results showed that calcium carbonate particles improved the properties of composites, such as biostimulation or adhesion capacity. In addition, fillers such as calcite and argonite were compared. Studies revealed that despite the smaller particle diameter and more uniform distribution in the PU matrix, the composite with argonite showed worse properties than those with calcite. In the work of Das et al. [8] a composite consisting of vegetable-oil-based hyper-branched polyurethane and rapeseed protein functionalized multi-walled carbon nanotubes was prepared. The results showed that the obtained composite rebuilt the bone in 93% after only 45 days. Composites made of polyurethanes and bioactive ceramics show some similarities to human bones. The HAp chemical structure is very similar to the mineral part of bone. The polymer matrix ensures adequate flexibility, hardness and compressive strength [9]. In addition, ceramic nanoparticles in the polymer matrix have good adhesion [10]. HAp is also responsible for bioactivity, which results in forming the apatite layer through ion-exchange reactions [9,10]. Another application of polyurethane foams is the development of composite bones. The PU foam structure resembles spongy bone, therefore, in order to restore the bone structure, the polyurethane foam was coated with the glass fibre reinforced epoxy resin to mimic the cortical bone. This composite exhibits very similar fatigue properties, Young's modulus, strength and hardness to natural bone [11,12].

The main goal of our research was to design and study the biodegradable PU-based composite scaffolds filled with β-TCP microparticles and hydroxyapatite (HAp) which can be applied as biomaterials in bone tissue engineering. The influence of β-TCP and HAp on mechanical and thermal properties, porosity, biodegradability and bioactivity of PU-based scaffolds was investigated.

Materials and Methods

Preparation of porous polyurethane-based composites

4,4'-diphenylmethane diisocyanate (MDI), poly(ethylene glycol) (PEG) with an average molar mass 2000 g/mol and 1,4-butanediol (BDO) were obtained from Sigma Aldrich company. β-TCP and HAp microparticles were produced by Fluka Chemie GmbH. It was assumed that the resulting foam should contain 40% of the soft segments (PEG). For this purpose, appropriate calculations were made and the amounts of substrates used are shown in TABLE 1.

$$m_{PEG} = x \cdot m_{PU}$$

where:
m_{PEG} - PEG mass [g],
x - PEG content,
m_{PU} - PU mass [g].

$$m_{MDI} = (m_{PU} - m_{PEG}) - m_{BDO}$$
$$R = M_i / f_i$$
$$m_{MDI} / R_{MDI} = m_{PEG} / R_{PEG} + m_{BDO} / R_{BDO}$$

where:
m_{MDI}, m_{PEG}, m_{BDO}, m_{PU} - masses of MDI, PEG, BDO and PU, respectively, [g]
R_{MDI}, R_{PEG}, R_{BDO} - equivalents of MDI, PEG, BDO, respectively, [g/mol]
M_{MDI}, M_{PEG}, M_{BDO} - molar mass, respectively: MDI, PEG, BDO, [g/mol]
f_{MDI}, f_{PEG}, f_{BDO} - number of active functional groups: MDI, PEG, BDO, respectively.

Polyurethanes were foamed using water. Polyurethane composite materials were obtained using the one-step bulk polyaddition method. In the first step, PEG was dried at the temperature 60-70°C under vacuum. Next, the proper amount of melted PEG was mixed with the TCP or HAp by sonication. The appropriate amounts of BDO and water were then added and mixed mechanically. Then the isocyanate was melted and preheated up to at 55-60°C and added into the previously prepared mixture. The reaction mixture was stirred intensively for one minute and next the foam growing was observed. Finally, the obtained foams were heated and conditioned for 24 h at 50°C.

The FTIR measurements were performed using a VARTEX 70 spectrometer, with the ATR attachment with diamond crystal, at room temperature in the range of 4000-550 cm^{-1} and at the 2 cm^{-1} resolution. The porosity was determined planimetrically, using the VHX 5000 digital microscope.

The DSC tests were performed using the DSC 1 differential scanning calorimeter from METTLER TOLEDO. The samples for DSC with mass ca. 4 ± 0.1 mg were placed in closed and pierced aluminium pans. The measurements were taken at the 10°C/min heating rate under a nitrogen atmosphere with the 30 ml/min flow rate. At the beginning the samples were heated form -90° up to 200°C, then cooled to -70°C and again heated up to 200°C.

The mechanical tests (static compression) were performed using ZWICK machine, in accordance with ISO 3167 on the cubic samples with dimensions 10x10x10 mm and at 2 mm/min speed. The results were the mean of three measurements.

The surface wettability analysis was performed using the DSA10 automatic drop analysis system. The obtained results are the mean of 5 measurements of distilled water drops with 15-25 µl volume range.

TABLE 1. Quantitative proportions of substrates for PU composites synthesis.

TCP [%]	PEG [g]	MDI [g]	BDO [g]	TCP [g]
0				-
2.5				0.5
5	8	10.45	2.91	1
10				2
20				4
HAp [%]	PEG [g]	MDI [g]	BDO [g]	HAp [g]
0				-
2.5				0.5
5	8	10.45	2.91	1
10				2
20				4

The chemical stability of the materials was determined by changes in pH and ionic conductivity of the water extracts in accordance with EN ISO 10993-13. The samples were placed in plastic containers with the sample to water ratio 1:10, and incubated for 8 weeks at 37°C. The pH and conductivity were measured each week.

The preliminary bioactivity assessment was performed in the simulated body fluid (SBF). The samples were incubated for 21 days at the constant temperature of 37°C, the SBF was replaced every 3 days. The changes occurring on the surface of the samples were observed using NOVA NANO SEM 200 scanning electron microscope equipped with EDAX EDS analyzer.

Results and Discussions

The FTIR spectra for obtained PUR composites are presented in FIG. 1.

In the unmodified polyurethane sample, the absorption bands were observed in the range of 3450-3300 cm^{-1}, which was characteristic for the N-H group stretching vibrations. The bands in the range of about 2900 cm^{-1} derived from stretching vibrations typical for CH$_2$. They were also present in the spectra of PU composites. At about 1520 cm^{-1} there were bands derived from secondary amide groups, and at 1240 cm^{-1} from the tertiary. The obtained results confirmed forming the urethane bonds during the polyurethane synthesis. In the range of about 1160-1040 cm^{-1} there was the triplet derived from the stretching vibrations of the C-O-C group in PEG [13].

With the addition of TCP, an increase in the band intensity around 1040, 600 and 550 cm^{-1} was observed. These were typical bands derived from the stretching and bending vibrations of PO$_4^{3-}$. An increase in the band intensity at 1040 cm^{-1} may be attributed to the overlapping of C-O-C group and those characteristic for the phosphate group originating from TCP. The absorption bands at ca. 1700 cm^{-1} came from the carbonyl group. There were no bands from isocyanate groups at ca. 2270 cm^{-1} that confirmed the complete reaction of isocyanate groups [13,14]. Moreover, for the composites with HAp no absorption bands from OH group at 3571 cm^{-1} were observed that suggest the chemical bonding of HAp with PU chains.
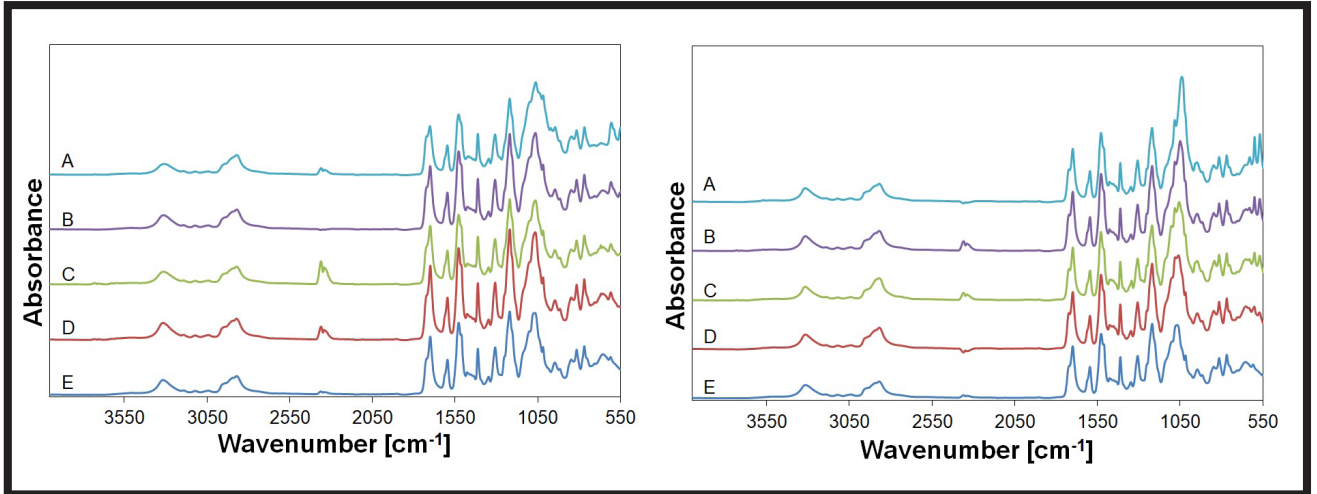
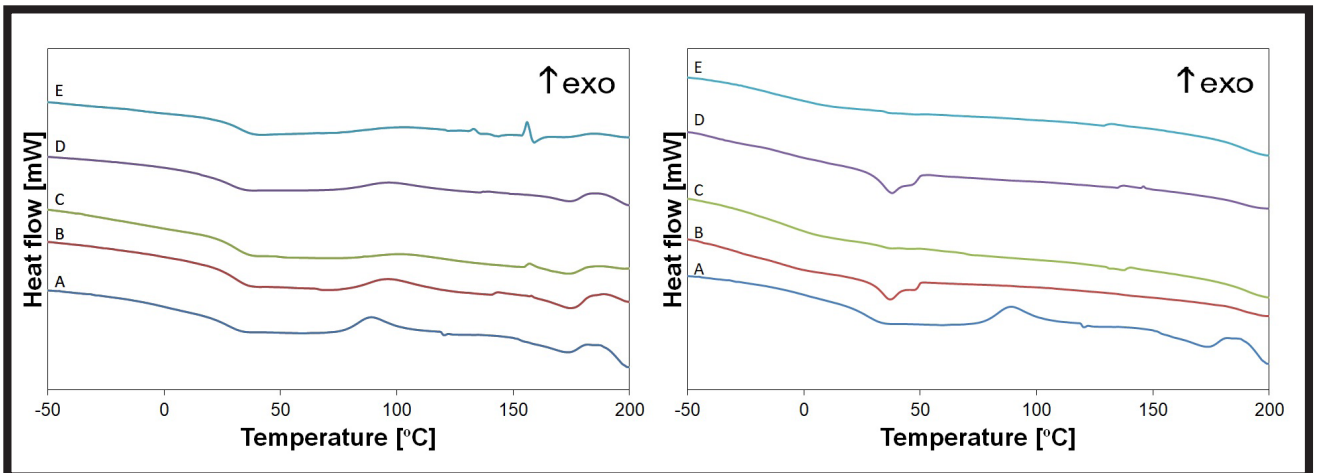**FIG. 1.** FTIR spectra for PU composites with TCP (left) and HAp (right): A) 0%, B) 2.5%, C) 5%, D) 10%, E) 20%.

FIG. 2. DSC curves from the second heating for PU composites with HAp (left) and TCP (right): A) 20%, B) 10%, C) 5%, D) 2.5%, E) 0%.

TABLE 2. DSC results: the melting temperature, glass transition and heat of fusion of obtained PU and PU composites.

Sample	Glass transition of soft segments		Glass transition of hard segments		Melting of soft segments		Cold crystallization		Melting of hard segments	
	T_g [ºC]	ΔC_p [kJ/molK]	T_g [ºC]	ΔC_p [kJ/molK]	T_{max} [ºC]	Heat of fusion [J/g]	T_{max} [ºC]	Heat of crystalliza-tion [J/g]	T_{max} [ºC]	Heat of fusion [J/g]
PU	-14	0.086	29	0.235	-	-	89	4.7	174	1.6
PU+2.5%HAp	-35	0.362	30	0.174	48	-	-	-	-	-
PU+5%HAp	-12	0.498	35	0.055	-	-	-	-	-	-
PU+10%HAp	-10	0.093	33	0.267	48	-	-	-	-	-
PU+20%HAp	-21	0.456	-	-	-	-	-	-	-	-
PU+2.5%TCP	-	-	30	0.345	-	-	96	5.6	175	4.5
PU+5%TCP	-	-	31	0.319	-	-	103	4.4	174	1.7
PU+10%TCP	-	-	27	0.328	-	-	97	5.0	175	2.0
PU+20%TCP	-	-	31	0.248	-	-	-	-	-	-

The DSC curves of the obtained composites are shown in FIG. 2 and the results are summarized in TABLE 2.

The DSC curves analysis of the unmodified polyurethane revealed two glass transitions: the first one at -13.6ºC with a ∆Cp equal to 0.086 kJ/molK derived from the soft segments, and the second one at 29.7ºC with a ∆Cp of 0.235 kJ/molK originating from the hard segments. Next, at 89ºC a broad exothermic peak was observed that could be attributed to the cold crystallization. The melting of hard segments was observed at ca. 160ºC. Analysing the DSC curves of the samples containing HAp, it was revealed that the glass transition of soft segments ranged from -35°C to -10ºC depending on the amount of HAp. Moreover, the incorporation of HAp only slightly changed the glass temperature of the hard segments.

For the composites with 2.5% and 10% HAp, the melting temperature of the soft segments was 48.3°C and 47.9ºC, respectively. This effect overlapped the changes in the baseline derived from the glass transition of the hard segments. Melting of the hard segments in the PU/HAp composites was not observed.

For the PU with TCP the glass transition temperatures for the hard segments were close to those of the samples containing HAp. The PU/TCP samples showed neither the glass transition for the soft segments nor their melting. On the other hand, the cold crystallization and melting were observed for the hard segments at a level similar to the unmodified polyurethane.

FIG. 3 presents the PU composites microphotographs and FIGs. 4-6 the pore size distribution in the PU composites.
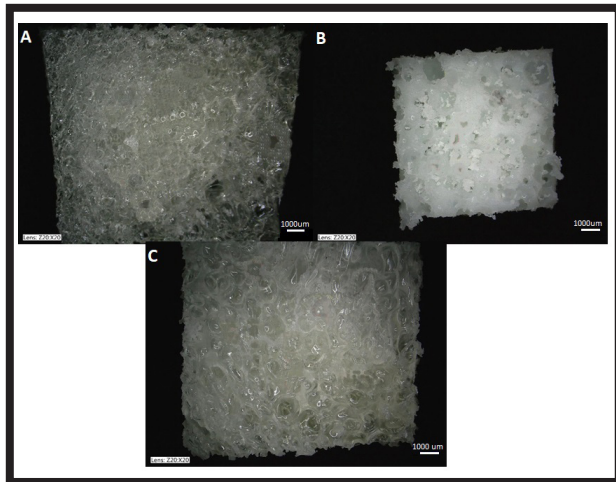
FIG. 3. Microphotographs of PU composites: unmodified PU (A), PU/10% HAp (B) and 10% TCP (C).
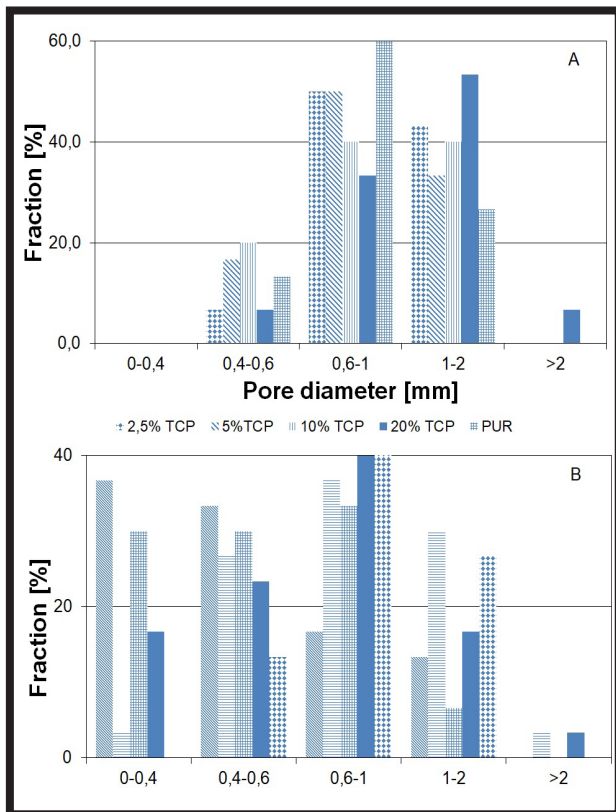
FIG. 4. Pore size distribution in composites with TCP (A) and HAp (B).
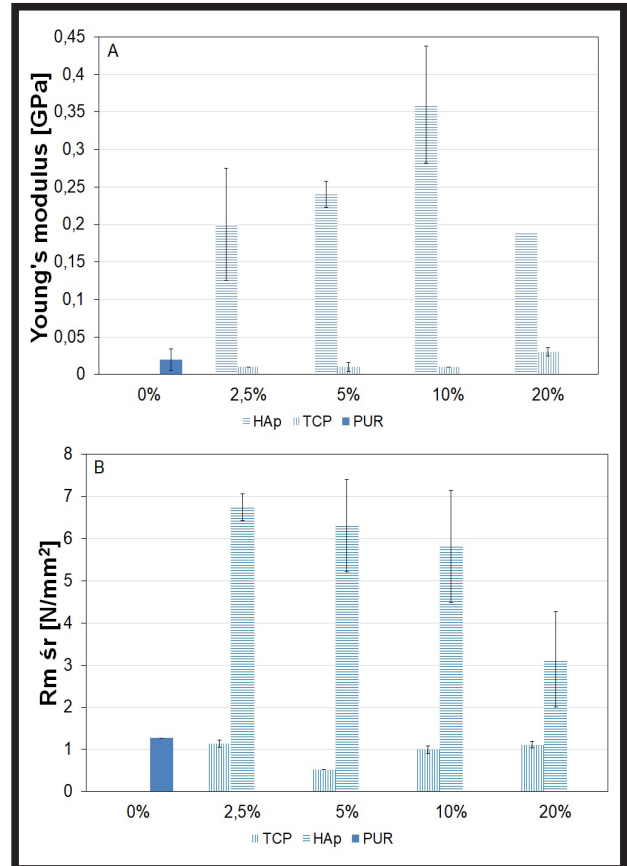
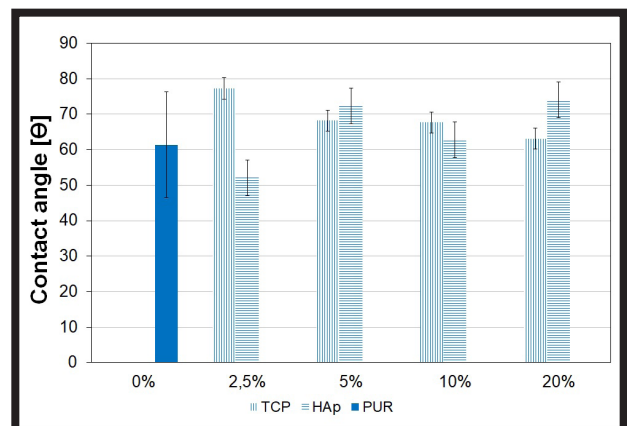**FIG. 5. Young's modulus for PUR with HAp, TCP (A) and compression strength for PU composites (B).**

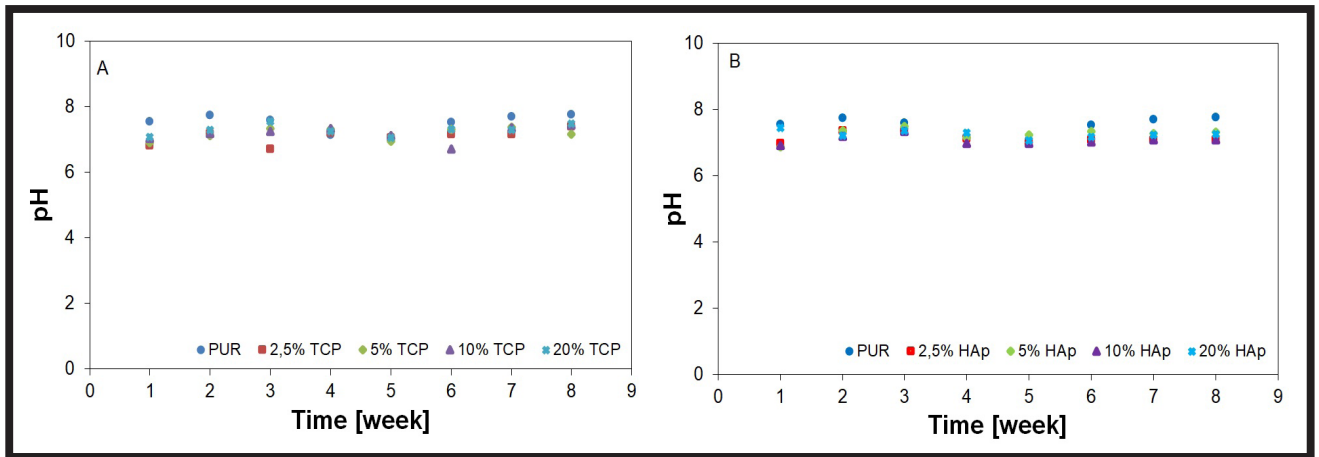**FIG. 6. Contact angle values for the samples tested.**

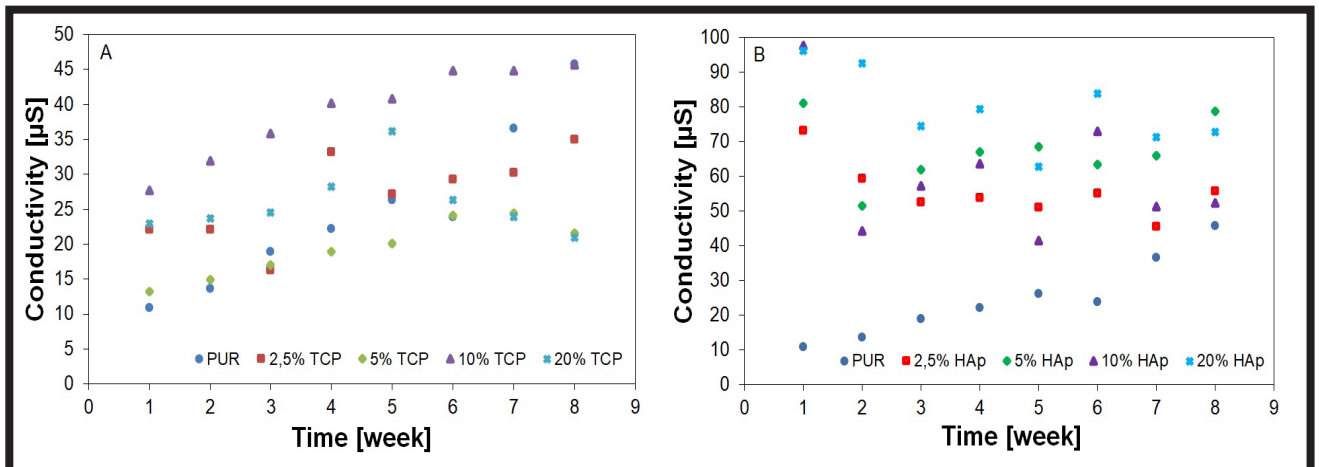**FIG. 7. pH vs. incubation time for PU/TCP (A) and PU/HAp (B) composites.**

FIG. 8. Conductivity vs. incubation time for PU/TCP (A) and PU/HAp (B) composites.

The composites with TCP revealed a higher number of pores with larger diameters, which is favourable for osteointegration. The highest number of pores in the 0-0.5 mm range was observed in the 10% TCP composite. In the PU/HAp composites, a high number of small pores was observed. The HAp incorporation significantly influenced the pore size distribution, even at the small Hap amount (2.5wt%), while the TCP incorporation led to significant changes in pore sizes at the higher TCP contents (20wt%). In all the samples, pores of 0.4-0.6 mm diameter were observed. Most of the smallest pores were observed in the PU/2.5% HAp. It can be concluded that the most favourable microstructure and pore size distribution was found in the PU/HAp composites [13,14].

In the next step, the mechanical properties were investigated. The compression tests results are presented in FIG. 7.

It was observed that only the addition of TCP did not change the PU composites compressive strength significantly. However, for the PU/HAp composites, the incorporation of 2.5% caused a significant increase in the compressive strength. Moreover, it was observed that the increasing HAp content resulted in the compressive strength decrease.

The wettability investigation showed that the contact angle of PU composites was in the range 50-80° - FIG. 6. In the case of the PU/TCP composites with the TCP content increasing, the contact angle diminished. On the other hand, for the PU/HAp composites, an opposite trend was observed.

During the incubation studies, the pH measurements showed that both the TCP and HAp incorporation only slightly decreased the pH of the unmodified PU and PU composites - FIG. 7. This effect can be explained by the slightly alkaline character of TCP and HAp. In the work by Szczepańczyk et al. the similar behaviour of the samples in the PBS and Ringer solutions was observed [13].

It can be seen that for the PU/TCP composites the highest conductivity of filtrates was observed for the PU/10% TCP - FIG. 8. Generally, the higher conductivity was observed for the PU composites when compared to the unmodified PU. With the bioceramics content increase, the conductivity increased due to the TCP and HAp slow dissolution.

In the next step, the preliminary assessment of bioactivity was performed using the Kokubo method [15]. Results of SEM-EDX observations are presented in FIGs. 9 and 10.

It was observed that the PU sample surface is strongly wrinkled and uneven with only sodium chloride crystals - no apatite crystals were found. Generally, the uniform distribution of TCP and HAp in the PU matrix was confirmed. In the PU/TCP composites, the apatites were not observed on the surface, and calcium phosphates were introduced as a filler. The PU/HAp composites revealed better bioactivity, a formation of the apatite layer was observed especially for the PU/5% Hap sample. This phenomenon can be explained by the nucleation effect of HAp on forming the apatite layer on the composite surface. A similar effect was observed by Szczepańczyk et al. [5,13] where incorporating HAp into the PU matrix increased the apatite formation in the SBF.
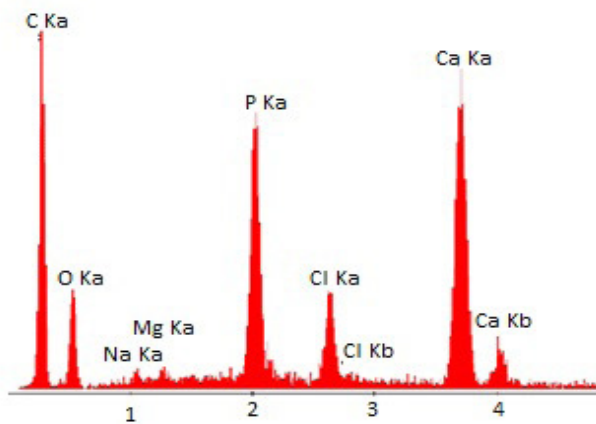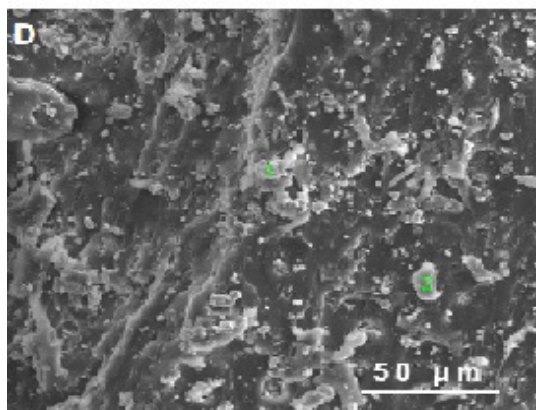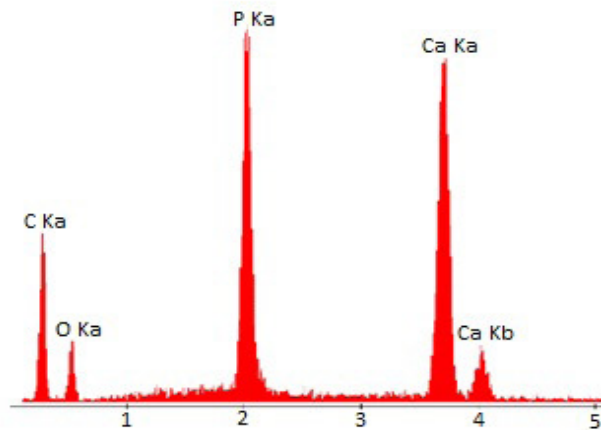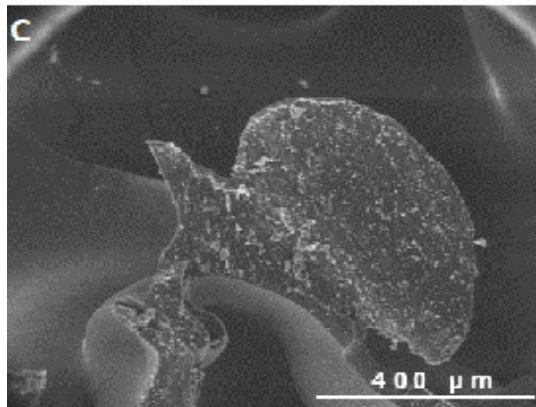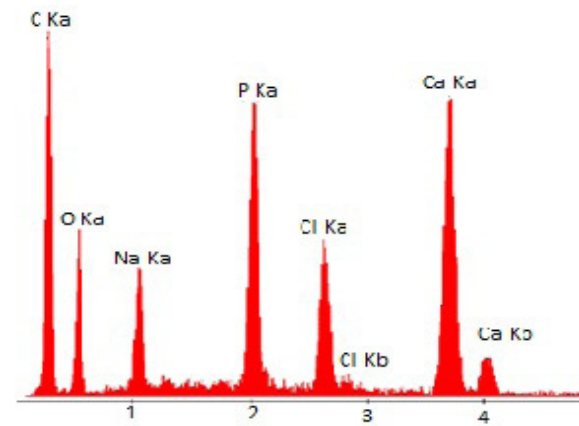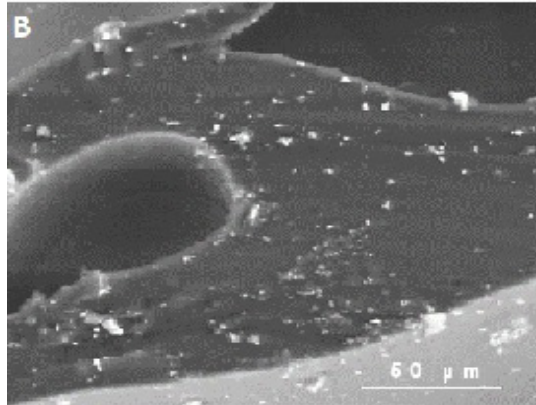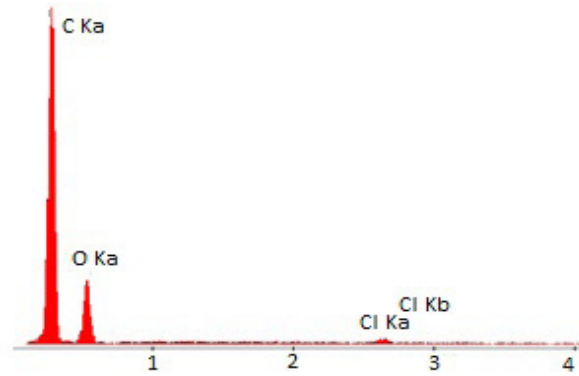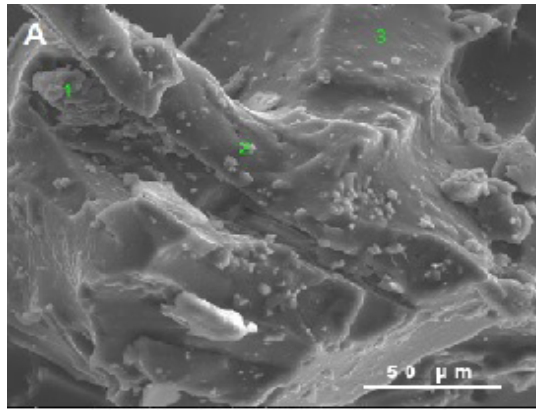
FIG. 9. SEM microphotographs and EDS analysis results for PU with: A) 2.5%, B) 5%, C) 10%, D) 20% TCP after incubation in SBF.
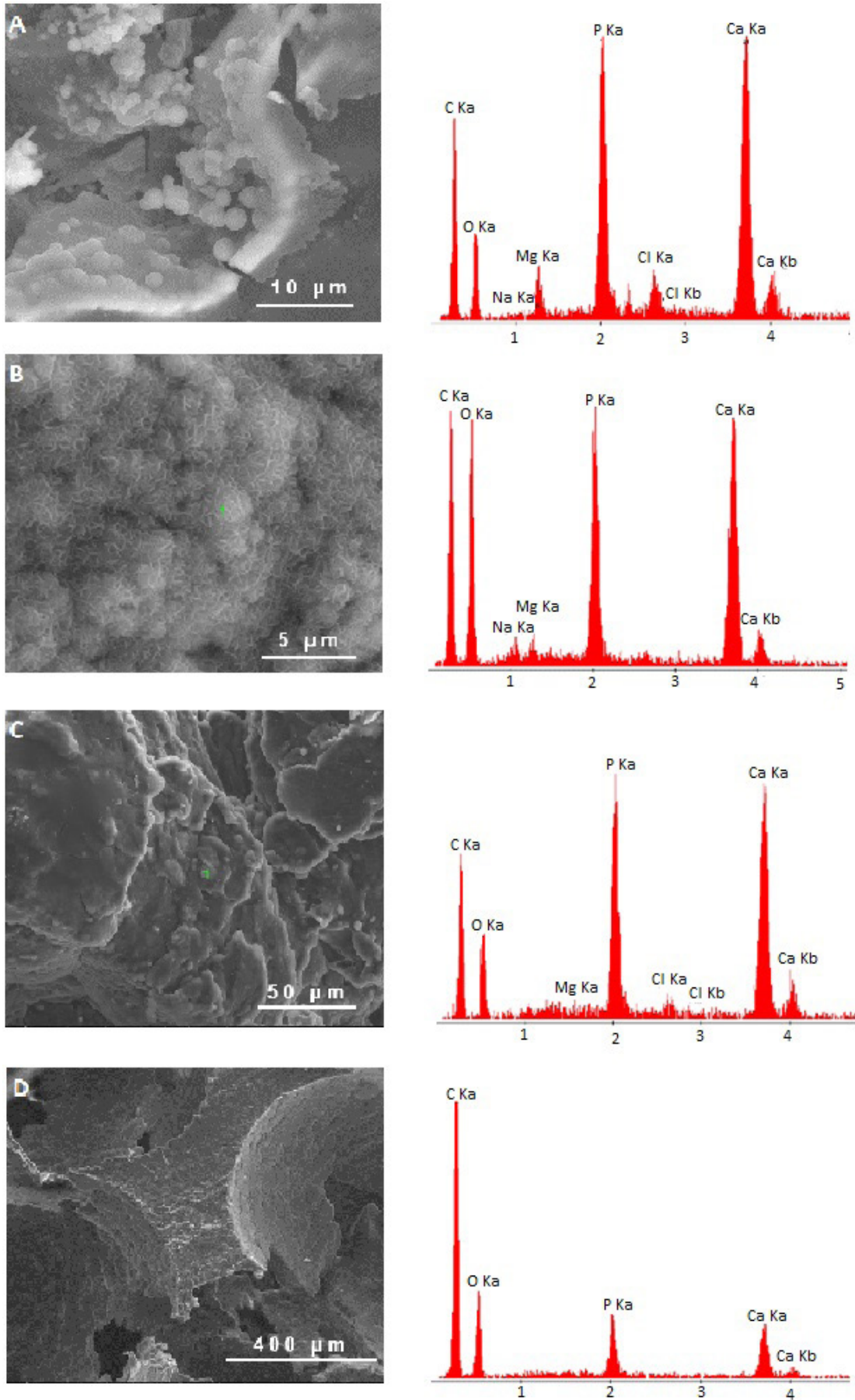
FIG. 10. SEM microphotographs and EDS analysis results for PU with: A) 2.5%, B) 5%, C) 10%, D) 20% HAp after incubation in SBF.

Conclusions

In this work, the PU composites enhanced with TCP and HAp were obtained and characterized. The FTIR results confirmed the polyurethane structure and the complete polyaddition reaction. Moreover, for the HAp composites, the absorption bands from the OH group were not observed at 3571 cm^{-1}, which suggests the chemical bonding of HAp with the PU chains. The porosity investigations of the obtained materials showed that the best pore distribution was found in the PU/HAp and PU/20% TCP composites. The SEM observations confirmed the uniform distributions of fillers in the composites. Moreover, the PU/HAp composites exhibited better bioactivity. The mechanical tests showed an increase in Young's modulus of the samples with hydroxyapatite and 20% TCP content. The chemical stability assessment confirmed the good hydrolytical stability of the composites in distilled water. The composites only slightly affected the pH of the environment and pH changes did not exceed 7.0 ± 0.8. The conductivity increased with higher amounts of ceramic additives. The results proved that the obtained composites possess some potential in orthopaedics.

ORCID iDs

P. Szatkowski: https://orcid.org/0000-0003-0861-6195
K. Pielichowska: https://orcid.org/0000-0002-5049-8869

References

[1] B. Świeczko-Żurek, A. Zieliński, i in.: Skrypt do przedmiotu biomateriały (2011).
[2] C. Turner and D. Burr: Experimental Techniques for Bone Mechanics, in Bone Mechanics Handbook, Second Edition, CRC Press (2001) 2-6.
[3] K.T. Łysiak-Drwal, Dominiak M., Malicka B.: Estimation of the influence of bone defects' dimensions on the healing outcome – 1-year observations. Stomatology 63 (2010) 365-376.
[4] B. Świeczko-Żurek: Biomateriały. Gdańsk (2009).
[5] L.P. Gabriel et al.: Bio-based polyurethane for tissue engineering applications: How hydroxyapatite nanoparticles influence the structure, thermal and biological behavior of polyurethane composites. Nanomedicine Nanotechnology, Biology and Medicine 13 (2017) 201-208.
[6] J.L. Ryszkowska, M. Auguścik, A. Sheikh, A.R. Boccaccini: Biodegradable polyurethane composite scaffolds containing Bioglass® for bone tissue engineering. Composite Science and Technology 70 (2010) 1894-1908.
[7] I. Dulińska-Molak, M. Lekka, K.J. Kurzydłowski: Surface properties of polyurethane composites for biomedical applications. Applied Surface Science 270 (2013) 553-560.
[8] B. Das et al.: Bio-functionalized MWCNT/hyperbranched polyurethane bionanocomposite for bone regeneration. Biomedical Materials 10 (2015) 1-16.
[9] J. Chlopek, P. Rosół, A. Morawska-Chochół: Durability of polymer-ceramics composite implants determined in creep tests. Composite Science and Technology 66 (2006) 1615-1622.
[10] K. Pielichowska: The influence of molecular weight on the properties of polyacetal/hydroxyapatite nanocomposites. Part 2. In vitro assessment. Journal of Polymer Research 19 (2012) 9788–1–9778–10.
[11] V. Shim and J. Boheme: Use of Polyurethane Foam in Orthopaedic Biomechanical Experimentation and Simulation (2012).
[12] A.R. Fariza, A. Zuraida, I. Sopyan: Application of Low Cost Polyurethane (PU) Foam for Fabricating Porous Tri-Calcium Phosphate (TCP). Journal of Biomimetics, Biomaterials, and Tissue Engineering 8 (2010) 1-7.
[13] P. Szczepańczyk, K. Pietryga, K. Pielichowska, J. Chłopek: Porous composites polyurethane/ß-TCP for orthopaedic applications. Engineering of Biomaterials 121 (2013) 33-41.
[14] M. Berdychowski: Zastosowanie modeli porowatych biomateriałów w procesach projektowania i symulacji (2014).
[15] T. Kokubo, H. Takadama: How useful is SBF in predicting in vivo bone bioactivity? Biomaterials 27 (2006) 2907-2915.